

We are IntechOpen, the world's leading publisher of Open Access books Built by scientists, for scientists

6,900

Open access books available

186,000

International authors and editors

200M

Downloads

Our authors are among the

154

Countries delivered to

TOP 1%

most cited scientists

12.2%

Contributors from top 500 universities



WEB OF SCIENCE™

Selection of our books indexed in the Book Citation Index
in Web of Science™ Core Collection (BKCI)

Interested in publishing with us?
Contact book.department@intechopen.com

Numbers displayed above are based on latest data collected.
For more information visit www.intechopen.com



General Cytotoxicity and Its Application in Nanomaterial Analysis

Magdalena Jedrzejczak-Silicka and Ewa Mijowska

Additional information is available at the end of the chapter

<http://dx.doi.org/10.5772/intechopen.72578>

Abstract

The recent increasing interest in the use of different nanoparticles in biological and medical applications encouraged scientists to analyse their potential impact on biological systems. The biocompatibility analyses of novel materials for medical applications are conducted using quantitative and qualitative techniques collected by the International Standards Organization (ISO). The well-known assays, such as tetrazolium-based assays used for mitochondrial function monitoring, LDH for membrane permeability determination and neutral red uptake (NRU) describing lysosome function, need to be optimised due to specific properties of wide range of nanomaterials. Physicochemical properties of nanoparticles (NPs) such as size, composition, concentration, shape and surface (e.g., charge, coating, aspect ratio), as well as the cell type play a crucial role in determining the nanomaterial toxicity (also uptake pathway(s) of NPs). Different nanomaterials exhibit different cytotoxicity from relatively non-toxic hexagonal boron nitride to rutile TiO₂ NPs that induce oxidative DNA damage in the absence of UV light. Finally, the results of the nanomedical analysis can be enriched by holographic microscopy that gives valuable information about the doubling time (DT), cell segmentation, track cell movement and changes in cell morphology. The results can be also completed by phenotype microarrays (PMs) and atomic force microscopy (AFM) techniques that fulfil experimental data.

Keywords: general cytotoxicity, nanomaterials, AFM analysis, holographic analysis, phenotype microarrays

1. Introduction

This chapter is dedicated to selected methods used to analyse the biocompatibility/cytotoxicity of different nanomaterials. The effect of nanomaterials on cellular metabolism and relative viability can differ according to their properties and experimental design. As shown by Frewin et al. [1],

biocompatibility analyses of novel materials for medical applications are conducted using quantitative and qualitative techniques. These techniques have been collected by the International Standards Organization (ISO) 10,993¹ (ISO-10993-1, 2009; ISO-10993-5, 2009; ISO-10993-6, 2007).

Nanotechnology and nanobiotechnology have focused scientists' attention in the last few years on their application in biomedical research, such as detecting and monitoring systems of cells within the body, delivery systems for various drugs, hyperthermia treatment, photodynamic therapy and tissue engineering [2]. The term 'nano' may be considered a different state of aggregation of matter in all its states—solid, liquid, gas and plasma [3].

The phenomenon of nanoparticles is based on their different physical (optical and electromagnetic), chemical (catalytic) and mechanical properties that depend on particle size, as well as surface and quantum effects. The surface effects manifest as scaling of physical properties (increased atomic fraction on particle surface compared to the interior), which includes increased chemical reactivity and reduced melting point of nanoparticles compared to larger particles of bulk material. NPs have a very large surface area in comparison to microparticles and larger materials, making this large surface area available for chemical reactions [4]. In addition, nanoparticles can be classified according to their composition (inorganic and organic, lipid-based and polymeric NPs), dimensionality, morphology, uniformity and agglomeration [Table 1] [3, 5]. Another classification divides nanomaterials into three groups: zero-dimensional materials (quantum dots), varying in shape and diameter; one-dimensional materials (nanorods and nanowires) and two-dimensional materials (nanobelts, nanodisks and nanosheets) [2].

The toxicity and cytotoxicity of nanomaterials are complex and depend on various factors, such as chemical composition, crystalline structure, size (at the nanolevel, the basic physicochemical properties of materials can change with variation in size) or aggregation. Nanomaterial composition determines its chemical interaction with cells, cellular uptake mechanisms and intracellular localisation. Chemical composition may also induce oxidative stress. For example, silver nanoparticle aggregates are more toxic than asbestos; CNTs are highly toxic and evoke much more damaging effect to the lungs than carbon black or silica NPs, but titanium oxide, iron oxide and zirconium oxide NPs are less toxic than asbestos [3, 6].

The crystalline structure effect of NP toxicity causes that some nanomaterials with a specific crystalline structure do not exhibit high toxicity, but other allotropes can strongly affect cell viability and exert an effect on human organism. Sato and co-workers [7] demonstrated that TiO₂ allotropes exhibited different toxicity. Rutile TiO₂ NPs (200 nm) induced oxidative DNA damage in the absence of UV light and also TiO₂ NPs (10–20 nm) stimulated reactive oxygen species (ROS) production under corresponding conditions; in contrast, anatase NPs of the same size did not cause this effect [3, 8, 9].

Another factor that determines nanomaterial toxicity is the size of NPs. In most cases, smaller nanoparticles are able to pass through physiological barriers. Small-size nanoparticles can

¹ISO-10993 ISO-10993-1 (ISO-10993-1 (2009) - Biological evaluation of medical devices — Part 1: Evaluation and testing within a risk management process; ISO-10993-5 (2009) - Biological evaluation of medical devices — Part 5: Tests for in vitro cytotoxicity; ISO-10993-6 (2007) – Biological evaluation of medical devices — Part 6: Tests for local effects after implantation

Classes	Types	Structure	Size	Properties
Carbon-based nanoparticles	Carbon nanotubes (CNTs)	Single-walled CNT (SWCNTs) Multi-walled CNT (MWCNTs)	Diameter between 0.4 and 100 nm; length between several nanometres up to centimetres	Improved compressive strength, tensile bending strength, flexural strength, durability, piezoelectric response, sensing ability
	Graphene (GF) and graphene oxide (GO)	Hydrophobic two-dimensional single monoatomic layers (GF) Oxidised form of GF (GO)	From 0.1 up to 300 μm	Large area; its surface can be easily functionalized with functional groups; ideal for high drug loading via π - π stacking, hydrophobic or electrostatic interactions; exceptional mechanical properties
	Nanodiamonds (ND)	Truncated octahedral structure	Diameter between 2 and 10 nm	Large area, enhanced biocompatibility, good mechanical strength, surface functionality, colloidal stability
Inorganic nanoparticles	Gold nanoparticles (GNPs, AuNPs)	Colloidal gold, nanorods, nanowires	Sizes of 1–100 nm	Absorb and scatter light; catalyst applications; anti-fungal, anti-microbial properties
	Silver nanoparticles (AgNPs)	Colloidal silver, spherical silver nanoparticles, diamond, octagonal, thin sheets	Diameter between 1 and 100 nm in size	Significant anti-microbial properties
	Iron oxide nanoparticles (IONPs)	Magnetite (Fe_3O_4); oxidised form maghemite ($\gamma\text{-Fe}_2\text{O}_3$)	Sizes of 1 and 100 nm	Superparamagnetic properties; the surface area-to-volume ratio is significantly high; higher binding capacity and excellent dispersibility
Mesoporous nanoparticles (MSN, MSNPs)	Nanosilica	Solid material with a porous, hexagonal, cubic and cage type	50–300 nm	Porous structure and large surface area; chemical stability; surface functionality and biocompatibility

Table 1. Types of nanomaterials [3, 5, 7].

enter cells by phagocytosis and other mechanisms (e.g., micropinocytosis, receptor-mediated endocytosis (RME) pathways mediated by caveolae, clathrin and caveolae/clathrin-independent endocytosis) [10, 11]. NP ability to enter the cells determines adhesive interactions, such as van der Waals forces, steric interactions or electrostatic charges [3, 12, 13]. Moreover, NPs smaller than 100 nm are not phagocytized as opposed to larger nanoparticles, but they enter via RME pathways [2, 11]. NP uptake can also occur in the absence of specific cell surface receptors. Nanoparticles smaller than 50 nm can easily enter most cells (with greater cytotoxicity),

while nanoscale devices smaller than 20 nm can cross blood vessels and cumulate in tissues [2]. Particles with larger surface area display tendency to agglomerate in the liquid, interact with molecules, such as proteins and DNA and may cause oxidation and DNA damage [3, 4, 14].

It is known that the shape (aspect ratio) also determines cellular uptake efficiency and may affect cell viability. Additionally, surface chemistry of nanomaterials modulates the response of biological systems and distribution in the organism. Surface functionalisation (with Fe_3O_4 , gold nanoparticles; type of bonding on the surface, e.g., covalent, noncovalent; dispersing agents, e.g., PEG) is a crucial factor that can significantly change the toxicity of NPs and prevent NPs from aggregating; it can also change their fate in biological systems [2, 3, 11]. For example, functionalization of MWCNTs with sodium sulfonic acid salt ($-\text{SO}_3\text{Na}$ or -phenyl- SO_3Na) increased their biocompatibility in comparison with unfunctionalised or carboxylic acid-functionalized ($-\text{COOH}$) MWCNTs [15]. Cellular uptake depends on different factors, such as nanomaterial and cell type, but also on environmental properties and the complexity of culture media. These specific conditions determine the aggregation process, which makes the interpretation of data on nanoparticle biodistribution or uptake difficult [3]. NP agglomerates affect and limit the direct extrapolation of *in vitro* data (providing a basis for understanding the mechanism of NP cytotoxicity and their uptake at the cellular level) to *in vivo* exposure [11, 16].

Intercellular localization of NPs and their interaction with cell components, such as the membrane, mitochondria, lysosomes and/or nucleus, are essential [11]. NPs can affect cell and organelle membranes, induce oxidative stress (ROS), DNA damage and mutagenesis and evoke apoptosis and protein up-/downregulation [11]; they can also modulate immune response [3, 17].

2. Nanoparticle cytotoxicity analyses and their limitations

The cytotoxicity study is an essential and crucial step in testing novel substances/nanomaterials in the context of biological and medical applications. Assays based on tetrazolium salts, like MTT (2-(4,5-dimethyl-2-thiazolyl)-3,5-diphenyl-2H-tetrazolium bromide), nitroblue tetrazolium (NBT) and the second-generation tetrazolium salts, such as XTT (sodium 2,3-bis(2-methoxy-4-nitro-5-sulfophenyl)-5-[(phenylamino)-carbonyl]-2H-tetrazolium inner salt), MTS (5-[3-(carboxymethoxy)phenyl]-3-(4,5-dimethyl-2-thiazolyl)-2-(4-sulfophenyl)-2H-tetrazolium inner salt) and WST-1 (sodium 5-(2,4-disulfophenyl)-2-(4-iodophenyl)-3-(4-nitrophenyl)-2H-tetrazolium inner salt) are basic tools for cytotoxicity determination, but nanomaterial testing is associated with certain challenges. The type of nanomaterials, manufacturing conditions, colloidal dispersion, chemical purity and photocatalytic activity of NPs may determine the usage of most traditional assays. Interactions between nanoparticles and molecules (i.e., reactants) used in well-established assays significantly affect the results and are one of the reasons of result variations [18, 19]. In assays based on colorimetric and fluorescence measurements, it has been found that nanomaterials, such as carbon nanotubes (CNTs), graphene/graphene oxide nanosheets, TiO_2 nanoparticles or boron nitride, interact with chromophore molecules, which may lead to false-positive results [19–21]. In other cases, the total surface area of NPs was sufficient to adsorb the reagent or fluorescent molecules, especially those with aromatic rings, which in turn led to false-negative results [21]. These results suggest

using alternative cytotoxicity assays based on tetrazolium salts, e.g., XTT, WST-1, INT or other assays that complement the analysis, e.g., Alamar Blue (AB), neutral red uptake (NRU) assay, LDH leakage assay, flow cytometry, cell death analysis (using trypan blue or annexin V/propidium iodide), protein concentration measurements using the Bradford assay, measurements of mitochondrial membrane permeability (MMP) or loss of glutathione (e.g., GSH) and the activation of proinflammatory cytokines (e.g., IL-6, IL-8 and/or TNF- α) [15, 19, 21].

A number of studies have been carried out to verify the effect of NPs on assay reagents [22]. Wörle-Knirsch and co-workers [23] indicated that CNT analysed using the MTT assay caused false-positive results due to the strong interaction between CNT and the insoluble formazan crystals [19, 23]. In the aforementioned study, SWCNTs were analysed on A549 (human alveolar epithelial cell line), ECV304 (endothelial cells derived from umbilical cord) and NR8383 (rat alveolar macrophage cell line) cell cultures and the results obtained in the MTT assay were verified by WST-1, LDH, mitochondrial membrane potential (MMP) and annexin V/PI analysis. The MTT assay indicated that SWCNTs affected cell viability, reducing it almost by 60% after a 24-h incubation period. Moreover, the decreased cell viability did not recover after longer incubation or higher concentrations of nanotubes. The results of the MTT assay were verified using WST-1, and no reduction in viability was detected. LDH and MMP assays confirmed WST-1 results, and flow cytometry using annexin V/propidium iodide showed lack of necrosis and/or apoptosis. Wörle-Knirsch et al. [23] concluded that nanotoxicological assays needed standardising with regard to the tested nanomaterial

Lupu and Popescu [24] used the MTT assay to evaluate TiO₂ toxicity. The effect of TiO₂ nanoparticles on living models is crucial due to their utilisation in food, beauty care and pharmacology industries. Additionally, TiO₂ nanoparticles are known to exhibit photocatalytic properties: the ability to catalyse redox reactions of molecules adsorbed on the surface during light exposition ($\lambda < 385$ nm). Photocatalytic reaction may occur by direct charge transfer of electrons (e^-) and holes (h^+) generated by light on the surface of titania nanoparticles. The reaction may be also mediated by reactive oxygen species (ROS), e.g., hydroxyl radicals ($\cdot OH$) or superoxide anions (O_2^-) formed at the interface of TiO₂ and water. Lupu and Popescu [24] clearly demonstrated that TiO₂ nanoparticles induced transformation of noncellular MTT to formazan. Formazan formation was found to be proportional to titania NPs, and this process was enhanced by daylight exposure. Moreover, the results obtained in the experiment without cellular model were validated using three cell lines—V79-4, HeLa and B16. The results demonstrated false viability that increased up to 14% for TiO₂ concentrations higher than 50 $\mu g ml^{-1}$ [24]. In addition, the TiO₂-MTT reaction was analysed in PBS environment. The reaction rate (formazan production rate) was proportional to TiO₂ and UV radiations (at 312 and 365 nm wavelengths) and inversely proportional to initial concentration of MTT. Moreover, reaction efficiency was enhanced by the presence of Na₂HPO₄ (phosphate concentration of 0.005 M for maximum efficiency), which is the basic component of PBS [25].

Casey et al. [26, 27] proved that single-walled carbon nanotubes (HiPco®) interacted with indicator dyes applied in Coomassie Blue, AlamarBlue™, neutral red uptake, MTT and WST-1 assays. In all cases, nanotubes interacted with dyes, which resulted in the reduction of the associated absorption/fluorescent emission. A spectroscopic study demonstrated that SWCNTs interacted with Coomassie and reduced the absorbance for all concentrations tested

(0.003–0.800 mgml⁻¹). As regards the AlamarBlue™ analysis (fluorescent measurements of all single-walled carbon nanotube solutions), quenching was monitored as a function of SWCNT concentration and plotted as an emission ratio at 595 nm by 540 nm excitation for the AB assay (5% solution of AB in culture medium) against SWCNT concentration. Another assay measuring NR uptake also showed SWCNT's ability to quench NR emission and was described as a function of SWCNT concentration. The MTT assay used in the cited study was found to interact with CNT. The reduction in MTT was associated with SWCNT concentration (absorption reduction was higher with increasing SWCNT concentration). For the WST-1 assay, it was concluded that the reduction in WST-1 absorbance was dependent on nanotube concentrations above 0.0125 mgml⁻¹. Casey et al. concluded that Coomassie, AB, NRU, MTT and WST-1 assays were not appropriate for the cytotoxicity analysis of carbon nanotubes [26, 27].

Limitations of MTT in cytotoxicity studies on graphene and graphene-related materials have been demonstrated in numerous publications. CCK-8 (tetrazolium-8-[2-(2-methoxy-4-nitrophenyl)-3-(4-nitrophenyl)-5-(2,4-disulfophenyl)-2H-tetrazolium] monosodium salt) assays are an attractive alternative for the MTT test. Evaluation of graphene adsorption was based on cell-free adsorptive experiments and demonstrated a gradual reduction of MTT to 93% during 2-h incubation, whereas CCK-8 was significantly reduced to 73% after exposure to graphene for 2 h. The intensity of graphene adsorption to MTT and CCK-8 was time-dependent. The quantity of the CCK-8 reagent absorbed by graphene was higher than that of MTT. It was reported that the π - π conjugated system of the CCK-8 molecule was much stronger than that of MTT due to three benzene rings and one five-membered heterocycle. MTT contains only two benzene rings and two five-membered heterocycles. Another reason for that process is that benzene ring groups strongly affect the adsorption. It was also noted that graphene can suppress the fluorescence effect caused by electron transfer from the dye molecule to the graphene surface. Although MTT and CCK-8 reagents are not fluorescent dyes, both of them display a positive electron on the molecules, similar to some known fluorescent dyes. Thus, it is possible that electron transfer occurs during the incubation with graphene and interferes with the dye molecule that contacts the enzymes. Jiao et al. noted that CCK-8 molecules can be more significantly disturbed by graphene than by the MTT reagent. Additionally, optical properties of graphene may also result in the loss of light signals used for detection in assays *in vitro* [28].

Cytotoxicity can also be determined using the lactate dehydrogenase (LDH) assay. The LDH assay is performed to exclude interactions between nanomaterials and fluorophore molecules [19]. The LDH assay, similar to the MTT assay, is a colorimetric method; thus, it can also interact with nanoparticles (e.g., CNT). Formazan crystals can be absorbed on the surface of MWNT (multi-walled nanotubes) through a strong π - π stacking interaction. The analysis of Ali-Boucetta et al. [19] proved that media containing the released LDH showed the same absorbance (at 490 nm) as MWNT:F127 (multi-walled nanotubes dispersed in the presence of Pluronic 127) dispersion in culture media. Ali-Boucetta et al. [19] proposed LDH assay modification that would eliminate the potential risk of interference of assay components with NPs (modified method vs. traditional procedure is presented in **Figure 1**).

In the experiment of Han et al. [29], copper (Cu-40), silver (Ag-35 and Ag-40) and titanium dioxide (TiO₂-25) were used to validate the popular assay. It was found that LDH was inactivated in

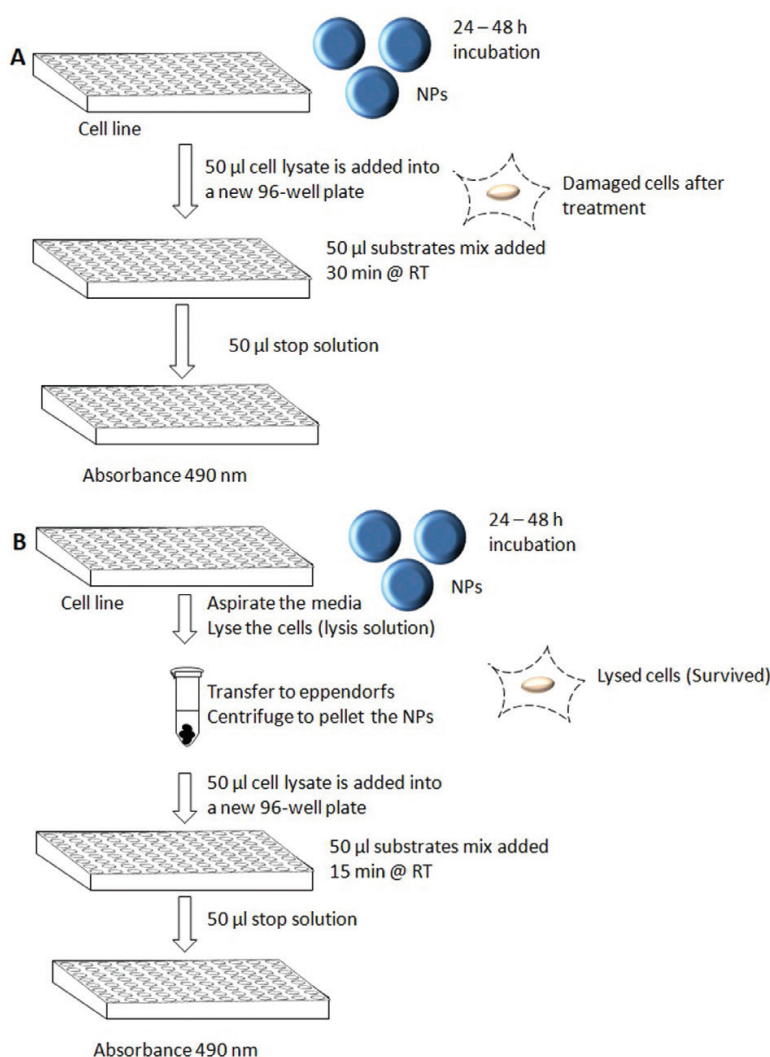


Figure 1. Schematic of the original (A) and modified LDH assay (B) [19].

the presence of Cu-40 and AG-35 in a dose-dependent manner. The effect of TiO₂-25 and Ag-40 NPs was not significant. In conclusion, these authors underlined the necessity to interpret the results with caution because of metal-catalysed oxidation [29].

Wang et al. [30] proposed modifying the LDH assay that would correct the erroneous results caused by potential interference of nanotubes with reporter chromophore, resulting in its adsorption on nanoparticle surface. The idea of this modification is based on the incubation of LDH derived from a known number of cells (e.g., DH82 macrophage cells) or a purified LDH standard (lactic dehydrogenase enzyme purified from rabbit muscle) with a precise amount (at different concentrations ranging from 5 to 100 μ gml⁻¹) of SWCNT or SWCNT-ox (carbon nanohorns). This additional procedure enables the quantification of the effects of NPs on the LDH level. The results obtained by Wang and co-workers clearly demonstrated that LDH concentrations decreased with increasing CNT concentration (at a wavelength of 490 nm). On the other hand, the 580 nm peak was elevated at the increased maximum absorbing wavelength. Based on the observation and regression analyses performed by Wang et al. [30], it was suggested that

LDH assay results should be verified by calibration curves in the presence of different SWCNT concentrations (in the range of 5–100 μgml^{-1}) at two wavelengths, 580 and 490 nm, for each LDH assay. This procedure more accurately determines cellular toxicity values [30].

Smith et al. [31] presented a simple protocol modification of the LDH analysis, which included membered additional conditional-specific controls. This modification enables accurate simultaneous measurement of the effects of death and growth inhibition. The additional step provides quantitative information that can be useful in applications such as drug discoveries [31]. Another approach in LDH assay analysis was proposed in the experiments of Chan et al. [32]. Modification of the LDH protocol allows to detect necrosis, including secondary necrosis [32].

In addition, calcein AM (CAM), Live/Death, neutral red, CellTiter®, Aqueous One (96 AQ), Alamar Blue (AB), CellTiter-Blue® (CTB), CytoToxOne™, and flow cytometry were used to determine their utility in nanoparticle toxicity evaluation. In the cited study, it was found that the results of the assay that depended on direct staining of cells were difficult to interpret, because of dye interactions with NPs. The 96 AQ assay proved optimal for NP analysis. The results were not significantly altered by interactions between the test factor and reagents in the assay [16].

Herzog et al. [33] suggested the clonogenic assay to determine real cytotoxic effect on cell cultures due to the false results (positive or negative) that may occur in NP testing. The clonogenic assay (colony formation assay) is based on the ability of a single cell to form a colony. The latter study was based on the ability of A549, BEAS-2B (normal human bronchial epithelial cells) and HaCaT (normal human keratinocytes) cells to form colonies after 7 (for HaCaT cells) and 10 (for A549 and BEAS-2B) days of incubation with SWCNT (HiPco®). The EC₅₀ comparison showed that the A549 cell line was more resistant than the other two lines. On the other hand, the analysis based on colony size showed that A549 was more sensitive than HaCaT cells. Although the clonogenic assay provided more accurate results than colorimetric tests, it did not become popular because it was too time-consuming for rapid toxicity screening [19, 33].

3. Difficulties in nanomaterial cytotoxicity analysis: Aggregates, protein corona and NP degradation

Nanomaterials are intensively studied as promising candidates for biomedical applications (e.g., targeted delivery of therapeutic drugs and medical imaging) with a purpose of eventual human administration [34]. NP design for medical applications should not only meet requirements, such as biocompatibility and biodegradability, but also site-specific delivery, long blood circulation and high cargo loading capacity [35]. Different nanomaterials show unique physical and chemical properties that depend, among others, on the type of materials (e.g., Au or Ag, Fe₃O₄, graphene and graphene oxide), hydrodynamic size, surface charge and aggregation behaviour and have been found to interact, often immediately (within seconds), after contact with biological systems, such as blood or tissue [34, 36, 37]. Nanoparticle aggregation via electrostatic screening can occur in complex aqueous mixtures of cell culture media that contain electrolytes, proteins, lipids and metabolites (highly ionic environment) [11, 38].

NPs at higher concentrations tend to form aggregates (agglomerates) under artificial conditions of *in vitro* cell cultures [16]. Many experiments found that NPs that form aggregates were not as cytotoxic as the same NPs at lower concentrations. Lower concentrations of NPs resulted in better internalisation and biodistribution in the circulatory system and organs [3]. Aggregation process is caused by magnetic attraction forces (types 1, 2 and 4), hydrophobic-hydrophobic interactions (for type 1) or hydrogen bonding between hydroxyl groups [39]. Different types of nanomaterials exhibit different tendency to form aggregates in PBS and culture media. CNTs have a strong tendency to agglomerate due to van der Waals interactions [40]. Metal oxides display higher tendency to form agglomerates in comparison to MWCNT. Metal oxides differ in size but were of similar size in PBS environment; thus, it was concluded that surface chemistry and/or the environment had a more significant effect on the aggregate formation process [14]. The size of aggregates may be dependent on the concentration and they tend to be slightly larger in culture media than in PBS. Moreover, monovalent and divalent cations may affect aggregate formation. Adsorption of media components, serum proteins and Ca^{2+} on nanoparticle surface determines NP aggregations and size distribution [14]. Agglomeration leads to cytotoxicity reduction, because of lower availability of inorganic NPs in contact with cells. In addition, the size of aggregates prevents their cellular internalisation [39]. Studies based on silica nanoparticles indicated that minimization of NP aggregation could be obtained by introducing an optimum balance of inert (e.g., methyl phosphonate) and active (e.g., hydroxyl and aldehyde) functional groups to the surface [41].

The protein layer of several nanometres on particle surface is called protein corona and it can be divided into a peripheral *soft* corona (SC)—dynamic protein exchanges with the surrounding medium—and a *hard* corona (HC)—a layer of more or less temporal constant composition (**Figure 2, Table 2**) [34, 42, 43]. In blood plasma, the surface of nanoparticles mainly adsorbs proteins, but some minor traces of lipids have also been found in the corona structure. Adsorption of proteins on the nanoparticle surface is the result of protein-nanoparticle binding affinities and protein-protein interactions. *Hard* corona interacts directly with the nanomaterial surface. *Soft* corona proteins interact with the hard corona via weak protein-protein interactions. Interestingly, the corona on the NP surface does not completely mask the nanomaterial surface or its functional groups [43]. The formation of protein corona and its thickness is a parameter that is also dependent on protein concentration, temperature, duration of particle-protein interaction, serum concentration and shear stress [34, 44].

Protein corona formation strongly affects cellular uptake mechanism, cell-nanoparticle interactions, intracellular location as well as cellular response (e.g., biocompatibility) [34, 35, 44]. The protein corona on the NP surface is hypothesised to hinder interactions of nanoparticle ligands and the targets on the cell surface [44, 47].

The study of Mirshafiee et al. [44] found that the protein corona formed on BCN-NPs (NPs functionalized with bicyclononyne) incubated in medium with 10% serum and 100% serum consisted of abundant proteins, such as chain A, a novel allosteric mechanism in haemoglobin, fetuin, haemoglobin foetal subunit beta or apolipoprotein A-II precursor. It was also reported that $\geq 88\%$ of proteins in BCN-NP coronas had a molecular weight below 30 kDa. Even relatively low molecular weight proteins created corona that significantly reduced NP

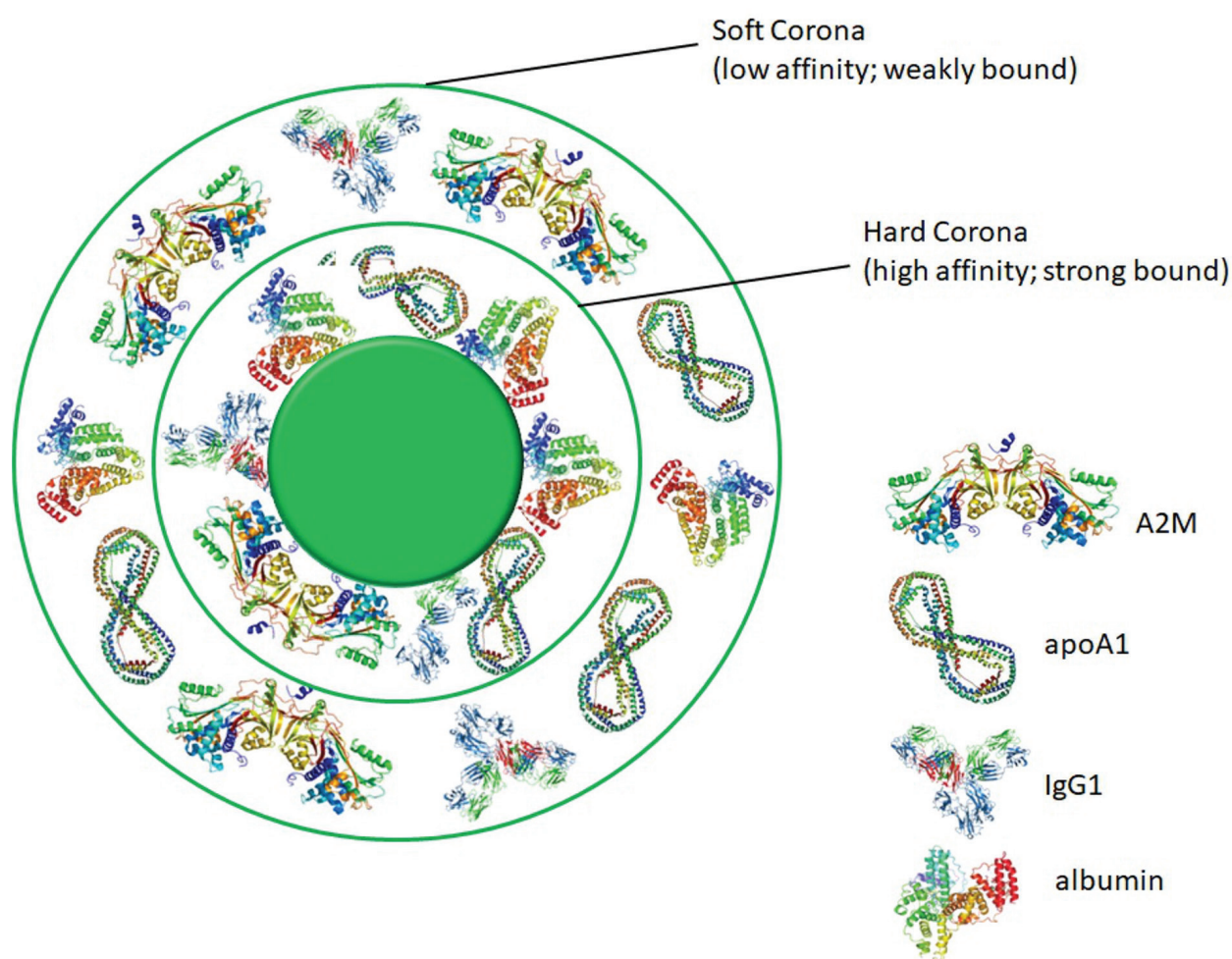


Figure 2. Structure of protein corona [34, 42, 43, 45].

targeting efficiency [44]. Single-walled carbon nanotubes (HiPco®) were also found to interact with cell culture medium and its components. Casey et al. described that SWCNT interacted with the medium via physisorption through van der Waals forces [26, 48].

The process of protein corona formation has a decisive influence on nanoparticle-induced toxicity. For example, silica nanoparticles (AmSil30) precoated with human plasma caused lower cell-death induction in primary human endothelial cells and microvascular endothelial cell line (ISO-HAS1). The resulting effect was dependent on the time of corona formation. The most significant effect was recorded for the early corona, but prolonged incubation with plasma (>30 min) did not counteract membered toxicity [49]. In another example, thrombocytes were used to study the protein corona effect on the biological model. In the latter study, nanoparticles exposed to human plasma for 0.5 min did not activate thrombocytes to form aggregates due to the presence of the plasma protein corona [49]. The impact of protein corona formation on cellular uptake and dispersion state of nanoparticles after exposure to plasma was also investigated. It was found that NPs were monodispersed after short-time exposure (<10 min), whereas aggregates started to form during prolonged exposure (>30 min), but the

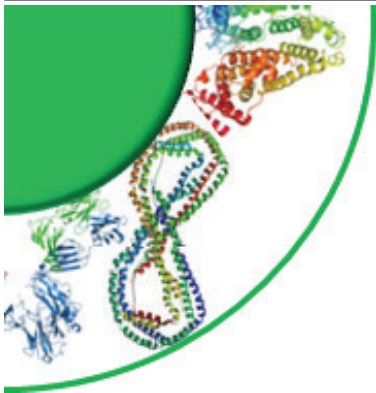
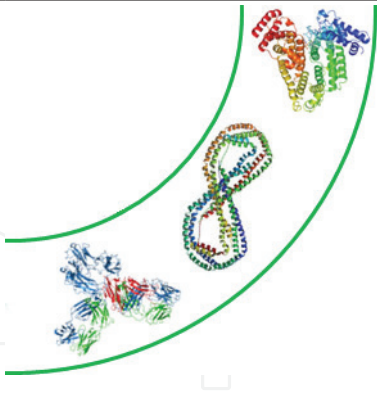
Hard corona	Soft corona
	
Tightly bound proteins	Loosely bound proteins
Large binding energy adsorption ($\uparrow \Delta G_{\text{ads}} $)	Low binding energy adsorption ($\downarrow \Delta G_{\text{ads}} $)
Lower dissociation rate of proteins with nanoparticles ($\downarrow k_{\text{off}}$)	Higher dissociation rate of proteins with nanoparticles ($\uparrow k_{\text{off}}$)
Directly interacting with surface of nanoparticles	Protein-protein interaction
Stable on nanoparticle surface; able to influence the functional response	Fleeting on nanoparticles; irrelevant for the functional response

Table 2. Characteristic features of hard (HC) and soft corona (SC) [46].

tendency to form aggregates was mostly dependent on physicochemical properties of NPs. However, Tenzer et al. [49] did not describe negative effects of AmSil30 precoated with the protein plasma corona. Biological effects of protein-NPs were analysed using two lines: HeLa and U937 [43, 50]. The study conducted by Maiorano et al. [50] demonstrated that AuNPs incubated in two different culture media (DMEM and RPMI) exhibited different protein coronas. RPMI-treated NPs had less prominent protein coronas and, as a consequence, induced stronger toxicity of HeLa and U937 cells [50]. The study of Gräfe et al. [34] reported that the presence of the protein corona reduced the interaction of human brain microvascular endothelial cells (HBMEC) with magnetic nanoparticles coated with PEI (polyethylenimine) during 30 min of incubation [34].

Nanoparticle-induced pathological effects, such as cell death, coagulation, thrombocytosis or cytotoxicity, are also dependent on the type of NPs, but selected cellular model is also crucial in this kind of experiments [49, 51]. For example, polystyrene-based NPs (PS) with different PS-COOH and PS-PO₃ groups coated with the serum protein were effectively taken up by both exposed cell lines (HeLa and hMSCs). NPs with PS-NH₂ and PS-SO₃ groups showed lower uptake by both cell lines [51].

The composition of protein corona was analysed using various methods and it was demonstrated that albumin, immunoglobulin G (IgG), fibrinogen and apolipoproteins were present in

the corona of all the analysed nanoparticles [43]. Corona identification and composition analysis (**Table 3**) provide not only information about its complexity, conditions of PC formation and physicochemical features but also data on toxicity, cellular interactions and uptake, targeting and finally the usefulness in nanomedicine [46].

For example, Urbas et al. [52] demonstrated that three types of nanoparticles, NPs-GO, Fe_3O_4 and $\text{GO-Fe}_3\text{O}_4$ displayed the ability to deplete various quantities of serum proteins from culture media (**Figure 3**). Graphene oxide and nanocomposite $\text{GO-Fe}_3\text{O}_4$ showed an increase in protein adsorption from culture medium. The results of the bicinchoninic acid (BCA) assay indicated different capacities of NPs to adsorb proteins in cell cultures [52].

Protein corona composition is also known to affect nanoparticle-cell interactions and biological fate of nanomaterials in cells. Gunawan and co-authors characterised the term ‘biological fate’ as describing the subcellular localisation of NPs and the distribution of NPs to specific organs *in vivo* [53]. An interesting study performed by Lesniak et al. [54] showed that silica (SiO_2) nanoparticles (50 nm) exposed to biological fluids (e.g., serum) mediated the interaction of NPs (at $100 \mu\text{g mL}^{-1}$ concentration) with A549 cells. Silica nanoparticles showed different degree and process of internalisation during incubation with the A549 cell line in complete (with 10% foetal bovine serum) and in serum-free medium. NP integration was higher in serum-free medium with accumulation in lysosomes and some of NPs localised free in the cytosol. On the contrary, NPs in complete medium (in the presence of a well-developed corona) were never observed free in the cytoplasmic matrix, but similar to serum-free medium, silica nanoparticles were found to accumulate in lysosomes. Lesniak et al. [54] observed that nanoparticles showed higher tendency to adhere to the cell membrane in serum-free conditions and concluded that the initial stronger adhesion could have partly contributed to higher uptake efficiency. Moreover, the presence of free NPs in the cytosol might be caused by perturbation of the early uptake pathway in cells exposed to serum-free medium (rather than an endogenously regulated cellular process) [53, 54].

Other results described various biological responses of different cell types to NPs with protein corona layers [53]. Single-walled carbon nanotubes preferentially bound IgM relative to IgG

Feature	Techniques for PC analysis
Isolation of NPs-PC	Centrifugation, size exclusion chromatography (SEC), magnetic separation/magnetic flow field fractionation (MgFFF)
PC structure analysis	Dynamic light scattering (DLS), differential centrifugal sedimentation (DCS), transmission electron microscopy (TEM)
Protein quantitation	Bicinchoninic acid (BCA) assay, Bradford assay, thermogravimetric analysis (TGA)
Binding affinity/stoichiometry and protein interaction	Fluorescence correlation spectroscopy (FCS), size exclusion chromatography (SEC), isothermal titration calorimetry (ITC), surface plasmon resonance (SPR), quartz crystal microbalance (QCM), Z-potential measurement, <i>in silico</i> simulation
PC composition	One-dimensional gel electrophoresis (1-DE or SDS-PAGE), two-dimensional gel electrophoresis (2-DE), mass spectrometry (MS)

Table 3. Analytical methods for corona evaluation [46].

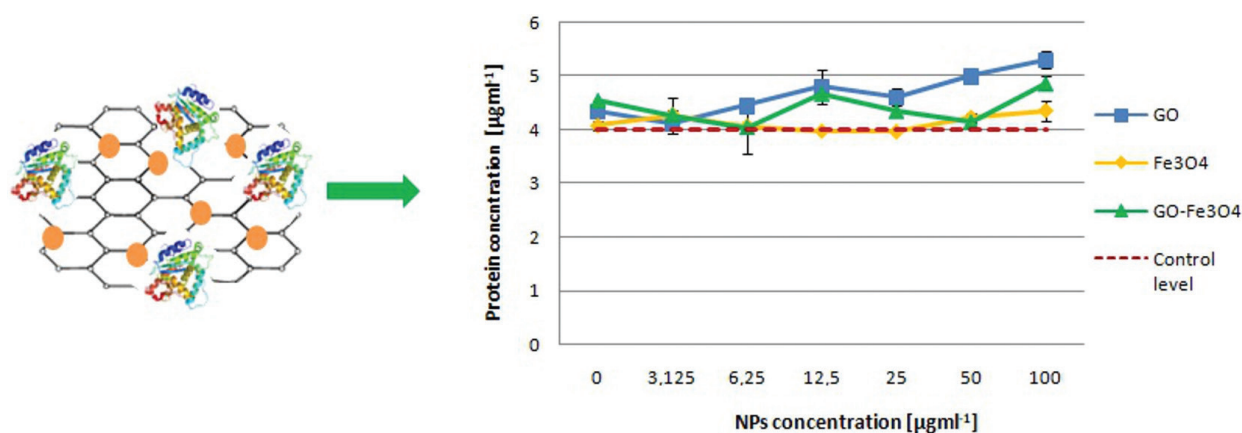


Figure 3. Protein adsorption onto tested NPs after 48-h incubation period in complete cell growth medium [52].

on PEG-SWCNTs due to the surface charge and the conformation of surface functional groups (PEG); this resulted in higher accumulation of the aforementioned NPs in the liver compared to the spleen [55]. Poly(D,L-lactide)-based NPs showed interaction of surface functional group (covalently conjugated with apoB₁₀₀ antibody) with LDL and were highly accumulated by liver macrophages [56]. Solid lipid nanoparticles (SLNs) modified with PEG induced the ABC phenomenon (accelerated blood clearance) upon repeated injections in mice and beagles. Moreover, PEGylated SLNs promoted liver/spleen uptake of NPs [57].

The application of polyethyleneglycol (PEG) for nanoparticle modifications reduces (but not totally suppresses) nonspecific protein corona formation [35, 51]. On the other hand, zwitterionic NPs were described to lack the protein corona [51].

The use of different nanomaterials for biomedical applications is indispensably associated with wide physico-chemical and biocompatibility analyses. The analysis of the effect of nanomaterials on different types of cells in various experimental conditions is an essential step in assessing the response of biological models (*in vitro* and/or *in vivo*) to direct contact with NPs [2]. On the other hand, cells/cell culture conditions as well as living system/biological fluids also affect morphological and physico-chemical properties of nanomaterials. Interesting results were obtained in the degradation process of sandwich-like mesoporous silica flake (mSiO₂) nanomaterial (developed as anticancer drug system) exposed to PSB solution for 24, 48 and 96 h. TEM analysis of mSiO₂ [Figure 4] showed that the porous structure of nanomaterial was degraded already after 24-h incubation in PBS [Figure 4a]. Another deformation found in mSiO₂ flake analysis was visible as large holes [Figure 4b-d]. The intensity of mesoporous silica flake degradation was time-dependent—the degree of deformation was associated with the size of holes formed in the nanoflake structure. The appearance of shapeless silica agglomerates was an additional result of the degradation process. Ninety-six-hour incubation caused deformation holes in silica nanoflakes that reached the point of total destruction of NPs [58].

Evidence of nanostructure biodegradation of the sandwich-like mesoporous silica flakes has also been confirmed in another study. After 48-h incubation, the whole surface of silica nanoflakes was covered with cavities and was entirely destroyed [59]. The mechanism of silica dissolution is based on two simultaneous processes—degradation and re-deposition of silica

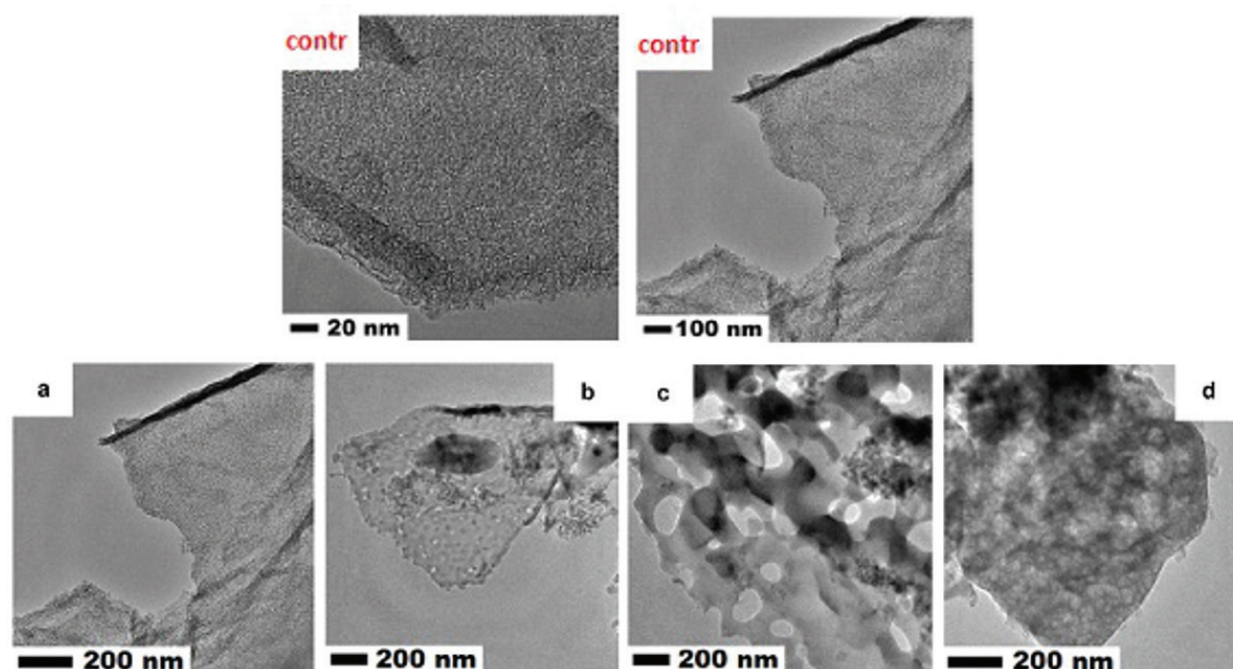


Figure 4. Transmission electron microscopy of mSiO₂ ('contr' – control sample) and mSiO₂ incubated in PBS, for 24 (a), 48 (b) and 96 h (c, d) [58].

on nanoparticle surface. Moreover, the effect of “self-healing” defects between both Si—O—Si bonds of double-linked Si atoms explains the very low rate of dissolution at the point of zero net proton charge (PZPC) of the surface [60].

A similar effect of PSB incubation on mesoporous silica nanospheres was observed by Yamada and co-workers [61], as these authors found that the mSiO₂ porous structure was degradable after 2-day incubation in PBS. After 3-day incubation, mSiO₂ displayed size and shape degradation with the final shape deformation and collapse of structures [61]. Another study based on core-shell magnetic mesoporous silica nanoparticles presented comparable results. Silica mesoporous hollow shells immersed in PBS for 2 days displayed structure deformation and additional cavities, whereas 8-day incubation showed complete degradation and coagulation resulting in new structure formation [62]. The erosion of mesoporous silica nanosphere structure modified with titanium dioxide was also observed in contact with *Streptomyces* cells. After 24-h incubation, mesoporous silica shell structure was degraded with simultaneous appearance of agglomerates, which clearly demonstrated that nanomaterial structure and composition could be affected by living cells [63].

4. Novel approaches in cytotoxicity studies

4.1. Phenotype arrays

Phenotype is the effect exerted by molecules (e.g., drugs, nanoparticles, etc.) on a cell, tissue or whole organism; thus, the phenotype screening provides a holistic analysis that usually is more

comprehensive than the sum of its parts. “*Phenomics*” is a part of complex technologies that also include transcriptomics, proteomics and metabolomics. PMs give a possibility to screen thousands of cellular phenotypes in real time [64].

Phenotype MicroArrays™ (PMs) are a combination of microplate reader (that can measure OD every 1 min over few hours and provide information about kinetics of carbon energy reactions in a selected cell model) and microscopic modules equipped with fluorescence, brightfield, colour brightfield and phase contrast microscopy (for scanning changes in cell morphology during experiments). Phenotypic assays deliver more information and provide better understanding of the metabolic and cytotoxic effect of test substances [65]. Multiplex arrays can generate information on the use of energy pathways (based on the application of different nutrition analyses, PM-M1 to M4), effects of ions (PM-M5), hormones, metabolic effectors (PM-M6 to M8) and anti-cancer agents (PM-M11 to M14) (**Table 4**), cell number, cell health (based on cell health monitoring using phase contrast microscopy and kinetic determination of cellular energy) and apoptotic induction (via cell subpopulation analysis—examination of the increase in circularity due to cell shrinkage and cytoplasm condensation and lower phase signal exhibition) [65]. PMs can be used in genotype/phenotype analyses, cell line characterisation, metabolic reprogramming, cellular phenotype stability, Warburg effect, cell differentiation or bioprocess development [64]. Well-characterised model cell lines (e.g., HepG2, C3A, Colo205, A549, PC-3, IMR90, HL-60 or CEM) with defined metabolic properties can be used with the PM system to determine specific effects of nanomaterials on selected cell lines and to accurately identify the mechanism involved in the NP effect (e.g., mitochondrial toxicology) on the living system [66]. Array wells coated with different substances and combined with the redox assay (MA or MB redox dyes to measure cell energy [NADH] changes) are used for phenotypic determination. Comparison of two cell lines is visualised by bioinformatic software that highlights differences in recorded phenotypes (**Figure 5**) [64, 67].

For example, Phenotype MicroArrays™ (PM-M TOX1 Plate Energetic Substrate Assay, 96-well microplate coated with eight different oxidisable carbon sources—each of the eight nutrition sources coated on one of eight rows on a microplate) give the possibility to screen cell-based energetic phenotype in a target cell model, for example, the MDA-MB-231 RFP breast cancer cell line, using different cellular nutrition sources (e.g., α -D-glucose, inosine, D-galactose, D-glucose-1-phosphate, xylitol, α -ketoglutaric acid, D,L- β -hydroxybutyric acid or pyruvic acid). This kind of multiplex analysis provides information on cell morphology, metabolic activity (metabolic pathway activity), sensitivity in response to particular energetic additives and the final cellular genetic background characterisation. The addition of an apoptotic agent (e.g., oridonin), chemical inhibitor or stimulator provides an opportunity to evaluate the potential mechanism regulating the energy pathway [65, 66]. Another example of PM application was presented by Bochner et al. [68]. Based on four phenotypic assays (PM-M1 to M4, containing 367 substrate nutrients), different human cancer cell lines, including HepG2/C3A, HepG2, Colo 205, A549, PC-3, HL-60 and CCRF-CEM and two murine white and brown adipocyte cell lines were analysed to determine energy-producing pathways. The results showed that human cancer cell lines exhibited distinct metabolic activity profiles. Moreover, white and brown adipocyte cell lines also had different profiles of energetic activity; metabolic fingerprints were established in all cell lines [68]. Similarly, human endothelial cells from the coronary artery

Phenotype MicroArrays™	Feature	Substrates/agents
PM-M TOX1 (Biolog)	Effect of a tested factor on energy production (mitochondrial toxicity)	Eight different carbon source: α -D-glucose, inosine, D-galactose, D-glucose-1-phosphate, xylitol, α -ketoglutaric acid, D,L- β -hydroxybutyric acid, pyruvic acid
PM-M1 (Biolog)	Energetic substrate array	Carbon and energy sources (simple sugars, polysaccharides, carboxylic acids): cyclodextrin, dextrin, glycogen, maltitol, maltotriose, D-maltose, D-trehalose, D-cellobiose, gentiobiose, D-glucose-6-phosphate, D-glucose-1-phosphate, L-glucose, D-glucose, 3-O-methyl-D-glucose, methyl-D-glucoside, D-salicin, D-sorbitol, N-acetyl-D-glucosamine, D-glucosaminic acid, D-glucuronic acid, chondroitin-6-sulphate, mannan, D-mannose, methyl-D-mannoside, D-mannitol, N-acetyl- β -D-mannosamine, D-melezitose, sucrose, palatinose, D-turanose, D-tagatose, L-sorbose, L-rhamnose, L-fucose, D-fucose, D-fructose-6-phosphate, D-fructose, stachyose, D-raffinose, D-lactitol, lactulose, α -D-lactose, melibionnic acid, D-melibiose, D-galactose, α -methyl-D-galactoside, N-acetyl-neuraminic acid, pectin, sedoheptulosan, thymidine, uridine, adenosine, inosine, adonitol, L-arabinose, D-arabinose, β -methyl-D-xylopyranoside, xylitol, myo-inositol, meso-erythritol, propylene glycol, ethanolamine D,L- α -glycerol-phosphate, glycerol, citric acid, tricarballic acid, D,L-lactic acid, methyl D-lactate, methyl pyruvate, pyruvic acid, α -keto-glutaric acid, succinamic acid, succinic acid, mono-methyl succinate, tricarballic acid, L-malic acid, D-malic acid, meso-tartaric acid, acetoacetic acid (a), γ -amino-N-butyric acid, α -keto-butyric acid, α -hydroxy-butyric acid, D,L- β -hydroxy-butyric acid, γ -hydroxy-butyric acid, butyric acid, 2,3-butanediol, 3-hydroxy-2-butanone, propionic acid, acetic acid, hexanoic acid
PM-M2 (Biolog)	Energetic substrate array	Carbon and energy sources/nitrogen sources (protein-derived nutrients, primarily amino acids, dipeptides): Tween 20, Tween 40, Tween 80, gelatin, L-alaninamide, L-alanine, D-alanine, L-arginine, L-asparagine, L-aspartic acid, D-aspartic acid, L-glutamic acid, D-glutamic acid, L-glutamine, glycine, L-histidine, L-homoserine, hydroxy-L-proline, L-isoleucine, L-leucine, L-lysine, L-methionine, L-ornithine, L-phenylalanine, L-proline, L-serine, D-serine, L-threonine, D-threonine, L-tryptophan, L-tyrosine, L-valine, Ala-Ala, Ala-Arg, Ala-Asn, Ala-Asp, Ala-Glu, Ala-Gln, Ala-Gly, Ala-His, Ala-Ile, Ala-Leu, Ala-Lys, Ala-Met, Ala-Phe, Ala-Pro, Ala-Ser, Ala-Thr, Ala-Trp, Ala-Tyr, Ala-Val, Arg-Ala (b), Arg-Arg (b), Arg-Asp, Arg-Gln, Arg-Glu, Arg-Ile (b), Arg-Leu (b), Arg-Lys (b), Arg-Met (b), Arg-Phe (b), Arg-Ser (b), Arg-Trp, Arg-Tyr (b), Arg-Val (b), Asn-Glu, Asn-Val, Asp-Ala, Asp-Asp, Asp-Glu, Asp-Gln, Asp-Gly, Asp-Leu, Asp-Lys, Asp-Phe, Asp-Trp, Asp-Val, Glu-Ala, Glu-Asp, Glu-Glu, Glu-Gly, Glu-Ser, Glu-Trp, Glu-Tyr, Glu-Val, Gln-Glu, Gln-Gln, Gln-Gly, Gly-Ala, Gly-Arg, Gly-Asn, Gly-Asp, α -D-glucose

Phenotype MicroArrays™	Feature	Substrates/agents
PM-M3 (Biolog)	Energetic substrate array	Carbon and energy sources/nitrogen sources (dipeptides): Gly-Gly, Gly-His, Gly-Ile, Gly-Leu, Gly-Lys, Gly-Met, Gly-Phe, Gly-Pro, Gly-Ser, Gly-Thr, Gly-Trp, Gly-Tyr, Gly-Val, His-Ala, His-Asp, His-Glu, His-Gly, His-His (c), His-Leu, His-Lys (d), His-Met, His-Pro, His-Ser, His-Trp, His-Tyr, His-Val, Ile-Ala, Ile-Arg (b), Ile-Asn, Ile-Gln, Ile-Gly, Ile-His, Ile-Ile, Ile-Leu, Ile-Met, Ile-Phe, Ile-Pro, Ile-Ser, Ile-Trp, Ile-Tyr, Ile-Val, Leu-Ala, Leu-Arg (b), Leu-Asn, Leu-Asp, Leu-Glu, Leu-Gly, Leu-His, Leu-Ile, Leu-Leu, Leu-Met, Leu-Phe, Leu-Pro, Leu-Ser, Leu-Trp, Leu-Tyr, Leu-Val, Lys-Ala (d), Lys-Arg (b), Lys-Asp, Lys-Glu, Lys-Gly, Lys-Ile (b), Lys-Leu (b), Lys-Lys, Lys-Met (e), Lys-Phe, Lys-Pro, Lys-Ser, Lys-Thr, Lys-Trp (b), Lys-Tyr (b), Lys-Val (d), Met-Arg (b), Met-Asp, Met-Gln, Met-Glu, Met-Gly, Met-His, Met-Ile, Met-Leu, Met-Lys (e), Met-Met, Met-Phe, Met-Pro, Met-Thr, Met-Trp, Met-Tyr, Met-Val, Phe-Ala, Phe-Asp, Phe-Glu, α -D-glucose
PM-M4 (Biolog)	Energetic substrate array	Carbon and energy sources/nitrogen sources (dipeptides): Phe-Gly, Phe-Ile, Phe-Met, Phe-Phe, Phe-Pro, Phe-Ser, Phe-Trp, Phe-Tyr, Phe-Val, Pro-Ala, Pro-Arg (b), Pro-Asn, Pro-Asp, Pro-Glu, Pro-Gln, Pro-Gly, Pro-Hyp, Pro-Ile, Pro-Leu, Pro-Lys (b), Pro-Phe, Pro-Pro, Pro-Ser, Pro-Trp, Pro-Tyr, Pro-Val, Ser-Ala, Ser-Asn, Ser-Asp, Ser-Glu, Ser-Gln, Ser-Gly, Ser-His (b), Ser-Leu, Ser-Met, Ser-Phe, Ser-Pro, Ser-Ser, Ser-Tyr, Ser-Val, Thr-Ala, Thr-Arg (f), Thr-Asp, Thr-Glu, Thr-Gln, Thr-Gly, Thr-Leu, Thr-Met, Thr-Phe, Thr-Pro, Thr-Ser, Trp-Ala, Trp-Arg, Trp-Asp, Trp-Glu, Trp-Gly, Trp-Leu, Trp-Lys (e), Trp-Phe, Trp-Ser, Trp-Trp, Trp-Tyr, Trp-Val, Tyr-Ala, Tyr-Gln, Tyr-Glu, Tyr-Gly, Tyr-His, Tyr-Ile, Tyr-Leu, Tyr-Lys, Tyr-Phe, Tyr-Trp, Tyr-Tyr, Tyr-Val, Val-Ala, Val-Arg, Val-Asn, Val-Asp, Val-Glu, Val-Gln, Val-Gly, Val-His, Val-Ile, Val-Leu, Val-Lys, Val-Met, Val-Phe, Val-Pro, Val-Ser, Val-Tyr, Val-Val, α -D-glucose
PM-M5 (Biolog)		Ions: NaCl, ammonium chloride, sodium selenite, potassium chloride, calcium chloride, manganese chloride, zinc chloride, copper (II) chloride, cobalt chloride, iodine, sodium phosphate, sodium sulphate, sodium molybdate, sodium tungstate, sodium orthovanadate, potassium chromate, sodium pyrophosphate, sodium nitrate, sodium nitrite, lithium chloride, ferric chloride, magnesium chloride
PM-M6 (Biolog)		Hormone and metabolic effectors: dibutyl-cAMP, 3-isobutyl-1-methylxanthine, caffeine, epinephrine, norepinephrine, L-leucine, creatine, triiodothyronine, thyroxine, dexamethasone, hydrocortisone, progesterone, β -estradiol, 4,5 α -dihydro-testosterone, aldosterone
PM-M7 (Biolog)		Hormone and metabolic effectors: insulin, resistin, glucagon, ghrelin, leptin, gastrin, exendin-3, hGH (somatotropin), IGF-I, FGF-1 (aFGF), PDGF-AB, IL-1 β , IL-2, IL-6, IL-8

Phenotype MicroArrays™	Feature	Substrates/agents
PM-M8 (Biolog)		Hormone and metabolic effectors: (Arg8) – vasopressin, parathyroid hormone, prolactin, calcitonin, calcitriol (1 α ,25-dihydroxyvitamin D3), luteinizing hormone (LH), luteinizing hormone releasing hormone (LH-RH), chorionic gonadotropin human (HCG), adrenocorticotrophic hormone human (ACTH), thyrotropic hormone (TSH), thyrotropin releasing hormone acetate salt (TRH), IFN- γ , TNF- α , adenosine, Gly-His-Lys acetate salt
PM-M11 (Biolog)		Anti-cancer agents: solasodine, rotenone, aklavine hydrochloride, deguelin(-), celastrol, juglone, sanguinarine sulphate, dactinomycin, methylmethane sulfonate, azathioprine, busulfan, aclarubicin, chloramphenicol, chloroquine diphosphate, cyclophosphamide, diethylcarbamazine citrate, emetine, fluorouracil, hydroxyurea, mechlorethamine, mercaptopurine, quinacrine hydrochloride, streptozosin
PM-M12 (Biolog)		Anti-cancer agents: tamoxifen citrate, thioguanine, acriflavinium hydrochloride, pentamidine isethionate, mycophenolic acid, aminopterin, berberine chloride, emodin, puromycin hydrochloride, neriifolin, 5-fluoro-5'-deoxyuridine, carboplatin, cisplatin, zidovudine (AZT), azacytidine, cycloheximide, azaserine, p-fluoro-phenylalanine, dimethylhydrazine hydrochloride, phenethyl caffeate (CAPE), camptothecin, amygdalin, ellagic acid
PM-M13 (Biolog)		Anti-cancer agents: monocrotaline, altretamine, carmustine, mitoxantrone hydrochloride, urethane, thiotepa, thiodiglycol, pipobroman, etanidazole, semustine, gossypol, formestane, ancitabine hydrochloride, nimustine, aminolevulinic acid hydrochloride, picropodo-phyllotoxin, beta-peltatin, perillyl alcohol, dibenzoylmethane, 6-amino nicotinamide, carmofur, indole-3-carbinol, rifaximin
PM-M14 (Biolog)		Anti-cancer agents: cepharanthine, 4'-demethyl epipodophyllotoxin, miltefosine, elaidyl phosphocholine, podofilox, colchicine, methotrexate, acivicin, floxuridine, lefunomide, rapamycin, 13-cis retinoic acid, all-trans retinoic acid, piceatannol, (+)-catechin, mitomycin C, cytosine-beta-D-arabinofuranoside, daunorubicin hydrochloride, doxorubicin hydrochloride, etoposide, nocodazole, quercetin dihydrate, vinblastine sulphate

Table 4. Array examples [65].

(HCAEC), umbilical vein (HUVEC) and normal lung fibroblasts (NHLFs) were selected for cellular metabolism monitoring also with the use of phenotypic assays (PM-M1 to M4). The results obtained in this study demonstrated that all three cell lines strongly utilised adenosine, inosine, D-mannose and dextrin. HCAEC also metabolised mannan, pectin, gelatine and tri-carballic acid, while the HUVEC cell line did not exhibit the ability to metabolise any other unique substrates. NHLFs were able to additionally utilise sugars and carboxylic acids [69].

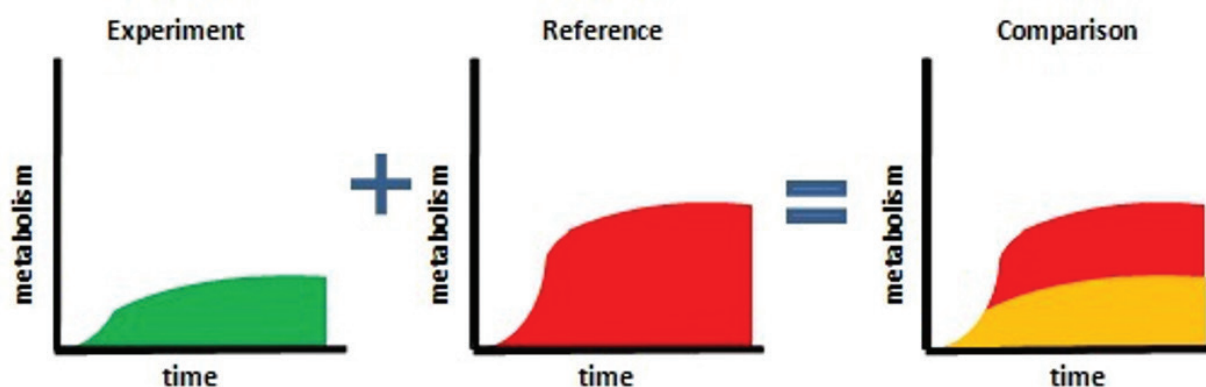


Figure 5. Schematic visualisation that highlights differences in recorded phenotypes [64].

The profiling of human normal and cancer cells was also conducted by Parmar et al. [70]. HEK293, OV90, TOV112D, KLE, MES-SA and SKBR cell lines were selected to determine differences in response to anti-cancer agents using PM (PM-M11 to M14) and the effect of these agents on the mTOR signalling pathway by measuring S6 kinase (S6K) level. From a wide range of anti-cancer drugs, celastrol was found to inhibit the growth of SKBR, MESA-SA and TOV11D and target the mTOR signalling pathway [70]. In another study, Martinez-Reyes et al. [71] reported that mitochondrial metabolism was necessary for histone acetylation, hypoxia-inducible transcription factor (HIF-1) activation and proliferation based on WT-POLG and DN-POLG-HEK293 cell lines [71].

The application of PMs in nanotechnology is only a matter of time, thanks to the efficient and rapid determination of precise sites and modes of action of the tested substances. PMs provide a possibility to compare specificities of the study agents (e.g., drug and nanomaterial-drug conjugates) and the effect of the agent and its side effects. Finally, the PM system can be used for drug interactions or drug-nanomaterial analysis [67, 72].

The limitations of large-scale phenotyping techniques, including PM analysis, are related to the characteristics of all cells. PMs will not reveal the phenotypes of all cells, because cells have many phenotypes that are dependent on their environments. Different cells are constantly adapting in various ways to culture (environment) changes by altering their gene-expression pattern, protein content, membrane and cytoskeleton constitution and surface receptors. Moreover, the PM system will likely not record phenotypes that specifically involve intracellular structures (e.g., cytoskeleton, organelles or surface structures). In addition, the effect of some genes might be cryptic and the function of those genes only occurs under highly specific conditions; thus, it cannot be always determined in conditions provided by PM cultures [73].

Another approach to phenotypic screening is focused on microarray-based three-dimensional (3D) systems. 3D culture models may better mimic the *in vivo* cellular microenvironment and may be critical for cell phenotypes [74]. It should also be mentioned that cell migration, compound-mediated cytotoxicity, cellular adhesion, proliferation and differentiation can also be evaluated using non-invasive, labelled-free xCELLigence system. Electrical impedance monitoring is based on a set of gold microelectrodes fused to the bottom surface of a microtitre plate

well. The magnitude of impedance is dependent on the number of cells, the size and shape of the cells and cell-substrate attachment quality; therefore, it gives the possibility to analyse the effect, for example, of nanomaterials on cell morphology, adhesion and biocompatibility [75].

4.2. Digital holography (DH) microscopy

Holographic (transmission) microscopy is a high-resolution imaging technique that provides label-free and non-invasive, non-phototoxic and non-destructive method for real-time live cell culture analysis [76]. This type of microscopy allows for quantitative and qualitative measurements of living cells (not only cultures of mammalian cells, but also protozoan, bacterial and plant cells) and collecting information about cell surface area, cell viability and morphological changes, such as differentiation, proliferation, motility, cell death, confluence or cell segmentation (calculated from a particular hologram) [77–80]. Traditional brightfield microscopy has some limitations, such as difficulties in visualising individual cells due to their low contrast properties, whereas DH microscopy provides possibility to determine cell number directly in cell culture vessels [81]. The size of the HoloMonitor™ M4 (Phase Holographic Imaging AB, Lund, Sweden) makes it possible to place it in a cell culture incubator, so that cell observations can be conducted over long periods of time without any changes in cell culture conditions [78]. Digital holographic microscopy also enables the formation of three-dimensional (3D) images of the observed objects.

The presented technique is based on the phase shift (φ) of the probing laser light (or other coherent light source) that can be reflected or transmitted through the monitored object. The illuminating light is split into two beams (differing in phase): an object beam and a reference beam [78, 81]. The reference beam remains undisturbed, while the object beam is shifted in phase by the object [79]. Next, the object beam is re-joined and interferes with the reference beam and creates a hologram that is recorded on a digital image sensor (CCD or CMOS) [77, 81]. The total phase shift can be translated into optical thickness (L) and depends on the physical thickness of the examined object, wavelength (λ) and refraction index (n). Optical thickness can be measured at nanometre resolution [78, 81].

Holographic phase imaging is an excellent tool for cell morphometric characterisation and cell migration studies. This technique has recently been applied in clinical diagnostics, e.g., screening for malaria infection of erythrocytes, cancer cell analyses or sperm quality [79]. Interest in the use of DH microscopy in research is constantly increasing. For example, Lajkó et al. [82] analysed the effect of a drug based on GnRH-III (gonadotropin-releasing hormone-III) on melanoma cells. Holographic phase imaging was used to visualise the migratory behaviour of melanoma cells in response to daunorubicin (Dau) coupled with GnRH-III and its derivatives (modified at position 4 with Lys(Ac) (conj1) or Lys(nBu) (conj2)). Cell migration analysis showed increased migration activity when cells were exposed to conj1, whereas conj2 decreased melanoma cell activity and exerted an immobilising effect on tumour cell spreading; thus, it was a better candidate for targeted tumour therapy [82]. Monitoring of HeLa cancer cells and MC3T3-E1 preosteoblast cells via holographic technique was also conducted by Peter et al. [78]. These authors evaluated cell movements and morphological parameters of cells in two experiments. In the first one, the HoloMonitor™ M4 was used to detect the effect of EGCg (green tea—epigallocatechin gallate) on HeLa cell motility. Time-lap images showed that migration, motility and the speed of motility were reduced after EGCg

was added to the culture. The second experiment involved MC3T3 plated on transparent titanate nanotubes (TNT) surface and the impact on adhesion and spreading process of the cells was demonstrated using the HoloMonitor. The authors have concluded that holographic digital microscopy is a useful tool for cellular behaviour analysis, but some limitations have also been found. Peter et al. [78] observed that under certain thicknesses, some parts of the cells (e.g., parts of the thin lamellipodium) slicked into the background surface. It was caused by the limited vertical resolution of the optical system [78].

In our study, the effect of the h-BN-Au nanocomposite on L929 and MCF-7 cell lines was analysed during 12-h incubation using the HoloMonitor™ M4. L929 cells did not show any significant differences in the presence of the nanocomposite and the doubling time (DT) value was similar to DT obtained in the control culture (**Figure 6**). The results obtained for the MCF-7 cell line incubated with h-BN-Au demonstrated a stronger effect on cells. The DT analysis using holographic technique indicated a high reduction of proliferation capacity (the DT value for the MCF-7 control sample was 25.95 h, whereas for experimental cultures, it was 469.9 h) [83].

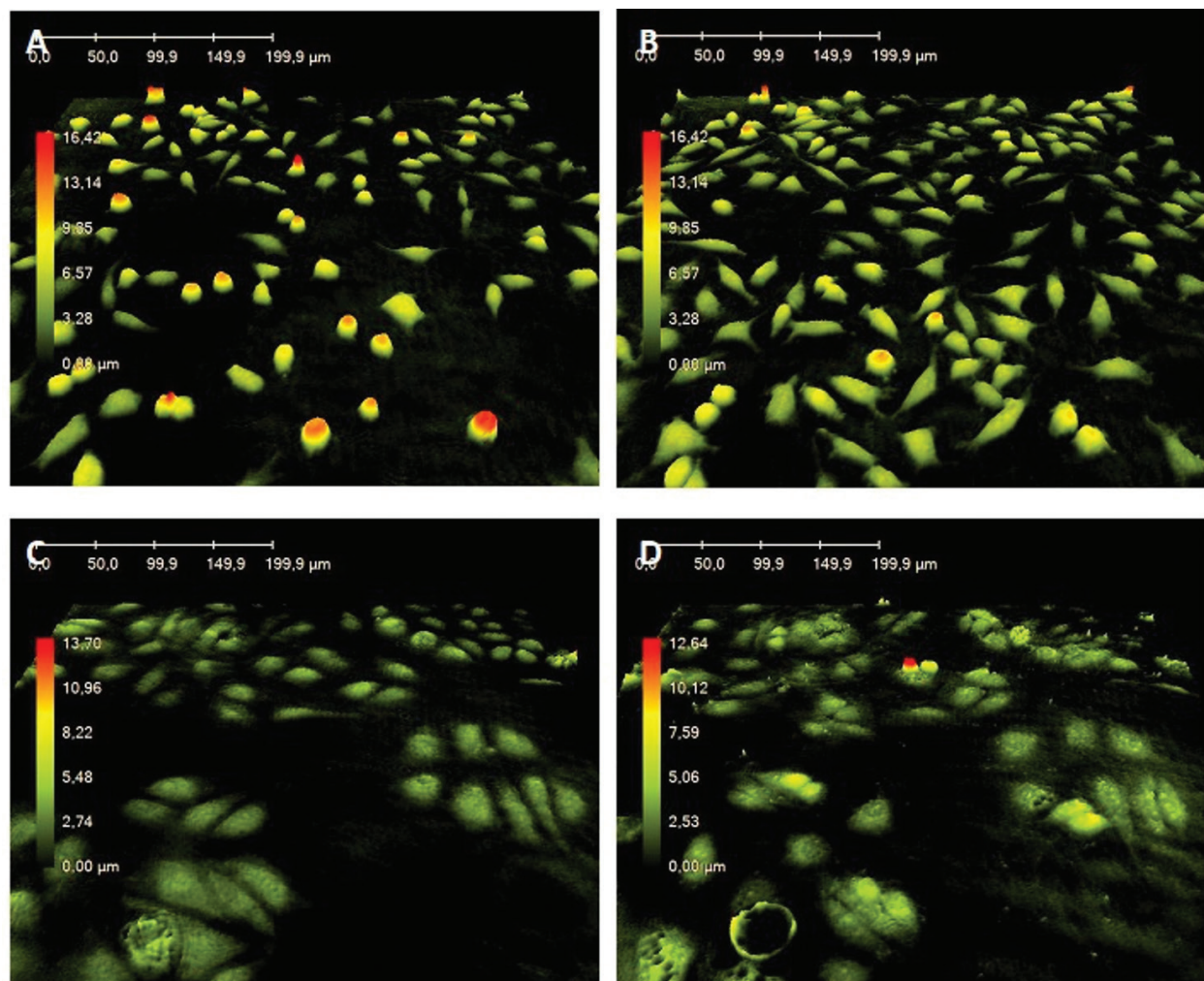


Figure 6. The morphology of the L929 and MCF-7 cell lines incubated with the h-BN-Au nanoparticles. L929 culture time-points at 0 h (A); at 12 h (B); MCF-7 culture time-points at 0 h (C); at 12 h (D) [83].

4.3. Atomic force microscopy (AFM)

Atomic force microscopy (AFM) is based on a laser reflected off a cantilever onto a scanning surface of the examined object and quantitative information about surface morphology and cell spread is collected.

AFM is a crucial technique for determining cell interactions on the surface of the tested material. If material exhibits high biocompatibility, the surface of the material will allow cells to attach (interaction between cell-surface integrin receptors) and adsorb extracellular matrix (ECM) proteins. Surface properties, such as wettability, roughness or surface charge, are important for cellular attachment and lamellipodium/filopodium formation. The AFM measurement provides information on cellular morphology changes and lamellipodium/filopodium permissiveness. The measurement of atomic force microscopy of living cells can be performed in PBS and provides information on cell height, total cell surface area, attachment angle and extension of lamellipodia/filopodia. It is also possible to measure fixed cell (in 4% paraformaldehyde) topography and examine filopodia and lamellipodia. An interesting example is the analysis of H4 and PC12 cell lines plated on different materials—glass, polystyrene (PSt), silicon (Si), nanocrystalline diamond (NCD) and cubic silicon carbide (3C-SiC). In the latter study, AFM analysis demonstrated that the type of the surface determined cell height/area, attachment angle and the reduction of the lamellipodium/filopodium area. Cell-substrate interaction was different for H4 and PC12 cell lines, e.g., for H4 cells; the most negative interaction was recorded for glass, the most positive for 3C-SiC, while PC12 cells had the most negative interaction with glass, but the best with 3C-SiC and PSt. The authors concluded that AFM analysis indicated that neural cell interactions with 3C-SiC resulted in the optimal cell viability, morphology and interaction of cells with 3C-SiC surface [1]. Frewin et al. [1] published the results of AFM analysis concerning cellular interaction on graphene. The experiments focused on cytoskeleton organisation and the determination of the number of contact sites, and AFM technology can provide valuable information on the mechanism of cellular adhesion and proliferation on graphene surface. Different methods of graphene preparation, for example, mechanical cleaving, chemical synthesis and chemical vapour deposition (CVD) on metals or epitaxial growth on SiC, not only give graphene different electrical, optical or morphological properties, but also different biocompatibility. For example, the biocompatibility of a single graphene layer produced by CVD on Cu was higher in comparison with SiO₂/Si surfaces studied on human osteoblasts and mesenchymal stem cells [1, 84]. In another study, epitaxially grown graphene films on (0001) 6H-SiC substrates were evaluated in cellular response experiments using AMF analysis. It was found that HaCaT (human keratinocytes) after 72-h culture on graphene and 6H-SiC surfaces exhibited similar morphology to cells cultured on the PSt control. On the other hand, the MTT assay suggested better biocompatibility for 6H-SiC than for the graphene surface. Moreover, different preparation of graphene surfaces (first one without any further surface treatment, and the second one additionally disinfected by immersion in ethanol) resulted in more homogeneous and increased cell adhesion on ethanol-sterilised graphene surface [1]. Our study also confirmed the undeniable value of AMF analysis in the experiment involving the MAC-T cell line seeded on different surfaces (glass, glass coated with poly-D-lysine) (**Figure 7**). In the aforementioned study, surface analysis and cell height analysis clearly exhibited differences in cell growth on the two surface variants [85].

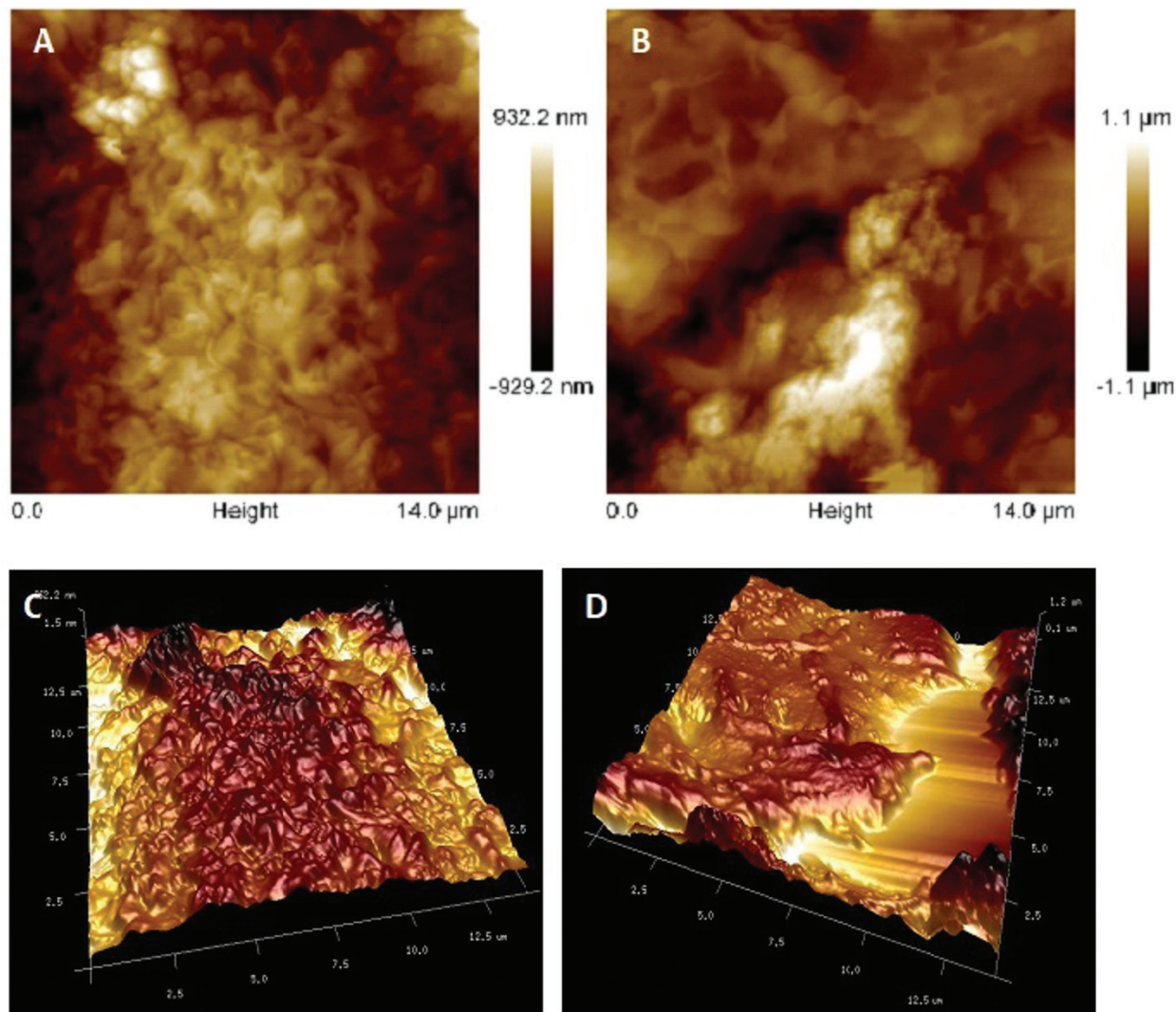


Figure 7. AFM analysis of MAC-T cells: cell height on glass surface (A); cell height on glass coated with poly-D-lysine (B); 3D image of cell growing on glass surface (C); 3D image of cell growing on poly-D-lysine (D) [85].

Another notable study used the AFM technique not only for cell analysis after nanoparticle uptake, but also after exposure to rotating magnetic field (RMF). Observations of MCF-7 cells after 1.5-h incubation in 40 mT magnetic field revealed changes in cell surface, which was rougher with many small pore-like structures in comparison to untreated cells [86].

5. Conclusions

The present overview describes and compares widely used biocompatibility/cytotoxicity assays in nanomaterial studies. Due to the type of nanoparticles and their properties, applicability of popular assays used for engineered nanomaterial screening might be limited. The significant numbers of false-positive or false-negative signals are generated [16]. The tendency of nanoparticles to:

- Interact and photocatalyse assay reagents,
- Create agglomerate in the conditions of in vitro and in vivo environment,
- Create protein layer of several nanometres on nanoparticle surface,
- Degrade and deform in vitro environment,

affect the results obtained in popular assays, thus classic cytotoxicity assays alone are not sufficient to evaluate nanomaterial biocompatibility.

Author details

Magdalena Jedrzejczak-Silicka^{1*} and Ewa Mijowska²

*Address all correspondence to: mjdrzejczak@zut.edu.pl

¹ Laboratory of Cytogenetics, West Pomeranian University of Technology, Szczecin, Poland

² Nanomaterials Physicochemistry Department, West Pomeranian University of Technology, Szczecin, Poland

References

- [1] Frewin CL, Oliverios A, Weeber E, Sadow SE. AFM and cell staining to assess the in vitro biocompatibility of opaque surfaces. In: Frewin CL, editor. *Atomic Force Microscopy Investigations into Biology—From Cell to Protein*. Rijeka: InTech; 2012. pp. 297-324. DOI: 10.5772/37078
- [2] Das S, Mitra S, Khurana SMP, Debnath N. Nanomaterials for biomedical applications. *Frontiers in Life Science*. 2013;**7**:90-98. DOI: 10.1080/21553769.2013.869510
- [3] Pacheco-Blandino I, Vanner R, Buzea C. Toxicity of nanoparticles. In: Pacheco-Torgal F, Jalali S, Fucic A, editors. *Toxicity of Building Materials*. Cambridge: Woodhead Publishing; 2012. pp. 427-475. DOI: 10.1533/9780857096357
- [4] Buzea C, Pacheco II, Robbie K. Nanomaterials and nanoparticles: Sources and toxicity. *Biointerphases*. 2007;**2**:MR17-MR71. DOI: 10.1116/1.2815690
- [5] Siafaka PI, Okur NÜ, Karavas E, Bikiaris DN. Surface modified multifunctional and stimuli responsive nanoparticles for drug targeting: Current status and uses. *International Journal of Molecular Science*. 2016;**17**:1440. DOI: 10.3390/ijms17091440
- [6] Nanotechnology in the Cement Industry—A Patent Analysis [Internet]. 2012. Available from: <https://www.nanowerk.com/spotlight/spotid=28101.php> [Accessed: 2017-09-22]
- [7] Sato K, Hosokawa K, Maeda M. Non-cross-linking gold nanoparticle aggregation as a detection method for single-base substitutions. *Nucleic Acid Research*. 2005;**33**:e4. DOI: 10.1093/nar/gni007

- [8] Gurr JR, Wang ASS, Chen CH, Jan KY. Ultrafine titanium dioxide particles in the absence of photoactivation can induce oxidative damage to human bronchial epithelial cells. *Toxicology*. 2005;**213**:66-73. DOI: 10.1016/j.tox.2005.05.007
- [9] Long TC, Saleh N, Tilton RD, Lowry GV, Veronesi B. Titanium dioxide (P25) produces reactive oxygen species in immortalized brain microglia (BV2): Implications for nanoparticle neurotoxicity. *Environmental Science and Technology*. 2006;**40**:4346-4352. DOI: 10.1021/es060589n
- [10] Hillaireau H, Couvreur P. Nanocarriers' entry into the cell: Relevance to drug delivery. *Cellular and Molecular Life Science*. 2009;**66**:2873-2896. DOI: 10.1007/s00018-009-0053
- [11] Alkilany AM, Murphy CJ. Toxicity and cellular uptake of gold nanoparticles: What we have learned so far? *Journal of Nanoparticles Research*. 2010;**12**:2313-2333. DOI: 10.1007/s11051-010-9911-8
- [12] Peters A, Veronesi B, Calderon-Garciduenas L, Gehr P, Chen LC, Geiser M, Reed W, Rothen-Rutishauser B, Schurch B, Schulz H. Translocation and potential neurological effects of fine and ultrafine particles—A crucial update. *Particle and Fibre Toxicology*. 2006;**3**:13. DOI: 10.1186/1743-8977-3-13
- [13] Geiser M, Rothen-Rutishauser B, Kapp N, Schurch S, Kreyling W, Schulz H, Semmler M, Im Hof V, Heyder J, Gehr P. Ultrafine particles cross cellular membranes by nonphagocytic mechanism in lungs and in cultured cells. *Environmental Health Perspectives*. 2005;**113**:1555-1560. DOI: 10.1289/ehp.8006
- [14] Sohaebuddin SK, Thevenot PT, Baker D, Eaton JW, Tang L. Nanomaterial cytotoxicity in composition, size, and cell type dependent. *Particle and Fibre Toxicology*. 2010;**7**:22. DOI: 10.1186/1743-8977-7-22
- [15] Schrand AM, Johnson J, Dai L, Hussain SM, Schlager JJ, Zhu L, Hong Y, Ōsawa E. Cytotoxicity and genotoxicity of carbon nanomaterials. In: Webster TJ, editor. *Safety of Nanoparticles*. Springer; 2009. pp. 159-187. DOI: 10.1007/978-0-387-78608-7_8
- [16] Monteiro-Riviere NA, Inman AO, Zhang LW. Limitations and relative utility of screening assays to assess engineering nanoparticle toxicity in a human cell line. *Toxicology and Applied Pharmacology*. 2009;**234**:222-235. DOI: 10.1016/j.taap.2008.09.030
- [17] Zolnik BS, Gonzales-Fernandez A, Sadrieh N, Dobrovolskaia MA. Nanoparticles and the immune system. *Endocrinology*. 2010;**151**:458-465. DOI: 10.1210/en.2009-1082
- [18] Berridge MV, Herst PM, Tan AS. Tetrazolium dyes as tools in cell biology: New insights into their cellular reduction. *Biotechnology Annual Review*. 2005;**11**:127-152. DOI: 10.1016/S1387-2656(05)11004-7
- [19] Ali-Boucetta H, Al-Jamal KT, Kostarelos K. Cytotoxicity assessment of carbon nanotube interaction with cell cultures. In: Hurst SJ, editor. *Biomedical Nanotechnology: Methods and Protocols, Methods in Molecular Biology*. New York: Springer; 2011. pp. 299-312. DOI: 10.1007/978-1-61779-052-2_19

- [20] Ciofani G, Danti S, D'Alessandro D, Moscato S, Mencassi A. Assessing cytotoxicity of boron nitride nanotubes: Interference with the MTT assay. *Biochemical and Biophysical Research Communications*. 2010;**394**:405-410. DOI: 10.1016/j.bbrc.2010.03.035
- [21] Al-Jamal KT, Kostarelos K. Assessment of cellular uptake and cytotoxicity of carbon nanotubes using flow cytometry. In: Balasubramanian K, Burghard M, editors. *Carbon Nanotubes: Methods and Protocols*. Stuttgart: Humana Press; 2010. pp. 123-134. DOI: 10.1007/978-1-60761-579-8_11
- [22] Monteiro-Riviere NA, Inman AO. Challenges for assessing carbon nanomaterial toxicity to the skin. *Carbon*. 2006;**44**:1070-1078. DOI: 10.1016/j.carbon.2005.11.004
- [23] Wörle-Knirsch JM, Pulskmap K, Krug HF. Oops they did it again! Carbon nanotubes hoax scientists in viability assays. *Nano Letters*. 2006;**6**:1261-1268. DOI: 10.1021/nl060177c
- [24] Lupu AR, Popescu T. The noncellular reduction of MTT tetrazolium salt by TiO₂ nanoparticles and its implication for cytotoxicity assays. *Toxicology in Vitro*. 2013;**27**:1445-1450. DOI: 10.1016/j.tiv.2013.03.006
- [25] Popescu T, Lupu AR, Raditoiu V, Purcar V, Teodorescu VS. On the photocatalytic reduction of MTT tetrazolium salt on the surface of TiO₂ nanoparticles: Formazan production kinetics and mechanism. *Journal of Colloid and Interface Science*. 2015;**457**:108-120. DOI: 10.1016/j.jcis.2015.07.005
- [26] Casey A, Herzog E, Davoren M, Lyng FM, Byrne HJ, Chambers G. Spectroscopic analysis confirms the interactions between single walled carbon nanotubes and various dyes commonly used to assess cytotoxicity. *Carbon*. 2007;**45**:1425-1432. DOI: 10.1016/j.carbon.2007.03.033
- [27] Casey A, Davoren M, Herzog E, Lyng FM, Byrne HJ, Chambers G. Probing the interaction of single walled carbon nanotubes within cell culture medium as a precursor to toxicity testing. *Carbon*. 2007;**45**:34-40. DOI: 10.1016/j.carbon.2006.08.009
- [28] Jiao G, He X, Li X, Qiu J, Xu H, Zhang N, Liu S. Limitations of MTT and CCK-8 assay for evaluation of graphene cytotoxicity. *RSC Advances*. 2015;**5**:532-540. DOI: 10.1039/C5RA08958A
- [29] Han X, Gelein R, Corson N, Wade-Mercer P, Jiang J, Biswas P, Finkelstein JN, Elder A, Oberdörster G. Validation of an LDH assay for assessing nanoparticle toxicity. *Toxicology*. 2011;**287**:99-104. DOI: 10.1016/j.tox.2011.06.011
- [30] Wang G, Zhang J, Dewilde AH, Pal AK, Bello D, Therrien JM, Braunschweig SJ, Marx KA. Understanding and correcting for carbon nanotube interferences with a commercial LDH cytotoxicity assay. *Toxicology*. 2012;**299**:99-111. DOI: 10.1016/j.tox.2012.05.012
- [31] Smith SM, Wunder MB, Norris DA, Shellman YG. A simple protocol for using a LDH-based cytotoxicity assay to assess the effects of death and growth inhibition at the same time. *PLoS One*. 2011;(11):e26908. DOI: 10.1371/journal.pone.0026908

- [32] Chan FK-M, Moriwaki K, De Rosa MJ. Detection of necrosis by release of lactate dehydrogenase (LDH) activity. *Methods in Molecular Biology*. 2013;**979**:65-70. DOI: 10.1007/978-1-62703-290-2_7
- [33] Herzog E, Casey A, Lyng FM, Chambers G, Byrne HJ, Davoren M. A new approach to the toxicity testing of carbon-based nanomaterials—The clonogenic assay. *Toxicology Letters*. 2007;**174**:49-60. DOI: 10.1016/j.toxlet.2007.08.009
- [34] Gräfe C, Weidner A, Lühe BC, Schacher FH, Clement JH, Dutz S. Intentional formation of a protein corona on nanoparticles: Serum concentration affects protein corona mass, surface charge, and nanoparticle-cell interaction. *International Journal of Biochemistry & Cell Biology*. 2016;**75**:196-202. DOI: 10.1016/j.biocel.2015.11.005
- [35] Palchetti S, Colapicchioni V, Digiacoio L, Caracciolo G, Pozzi D, Capriotti AL, La Barbera G, Laganà A. The protein corona of circulating PEGylated liposomes. *Biochimica et Biophysica Acta*. 2016;**1858**:189-196. DOI: 10.1016/j.bbame.2015.11.012
- [36] Del Pino P, Pelaz B, Zhang Q, Maffre P, Nienhaus GU, Parak WJ. Protein corona formation around nanoparticles—From the past to the future. *Materials Horizons*. 2014;**1**:301-313. DOI: 10.1039/C3MH00106G
- [37] Zhang Y, Wu C, Guo S, Zhang J. Interactions of graphene and graphene oxide with proteins and peptides. *Nanotechnology Review*. 2013;**2**:27-45. DOI: 10.1515/ntrev-2012-0078
- [38] Vesaratchanon S, Nikolov A, Wasan DT. Sedimentation in nano-colloidal dispersions: Effects of collective interactions and particle charge. *Advances in Colloid and Interface Science*. 2007;**134-135**:268-278. DOI: 10.1016/j.cis.2007.04.026
- [39] Díaz B, Sánchez-Espinel C, Arruebo M, Faro J, de Miguel E, Magadán S, Yagüe C, Fernández-Pacheco R, Ibarra MR, Santamaría J, González-Fernández A. Assessing methods for blood cell cytotoxicity responses to inorganic nanoparticles and nanoparticles aggregates. *Small*. 2008;**4**:2025-2034. DOI: 10.1002/sml.200800199
- [40] Fraczek-Szczypta A, Menaszek E, Blazewicz S. Some observation on carbon nanotubes susceptibility to cell phagocytosis. *Journal of Nanomaterials*. 2011:1-8. ID 473516. DOI: 10.1155/2011/473516
- [41] Bagwe RP, Hillierd LR, Tan W. Surface modification of silica nanoparticles to reduce aggregation and nonspecific binding. *Langmuir*. 2006;**22**:4357-4362. DOI: 10.1021/la052797j
- [42] Mahmoudi M, Lynch L, Ejtehadi MR, Monopoli MP, Bombell FB, Laurent S. Protein-nanoparticle interactions: Opportunities and challenges. *Chemical Reviews*. 2011;**111**:5610-5637. DOI: 10.1021/cr100440g
- [43] Rahman M, Laurent S, Tawil N, Yahia L, Mahmoudi M, editors. Nanoparticle and protein corona. In: *Protein-Nanoparticle Interactions. The Bio-Nano Interface, Springer Series in Biophysics*. Berlin: Springer; 2013. pp. 21-44. DOI: 10.1007/978-3-642-37555-2_2
- [44] Mirshafiee V, Mahmoudi M, Lou K, Cheng J, Kraft ML. Protein corona significantly reduces active targeting yield. *Chemical Communications*. 2013;**49**:2557-2559. DOI: 10.1039/c3cc37307j

- [45] Fleischer CC, Payne CK. Nanoparticle-cell interactions: Molecular structure of the protein corona and cellular outcomes. *Accounts of Chemical Research*. 2014;**47**:2651-2659. DOI: 10.1021/ar500190q
- [46] Pederzoli F, Tosi G, Vandelli MA, Belletti D, Forni F, Ruozi B. Protein corona and nanoparticles: How can we investigate on? *WIREs Nanomed Nanotechnology*. 2017;**9**: e1467. DOI: 10.1002/wnan.1467
- [47] Mahon E, Salvati A, BaldelliBombelli I, Lynch I, Dawson KA. Designing the nanoparticle-biomolecule interface for targeting and therapeutic delivery. *Journal of Controlled Release*. 2012;**161**:164-174. DOI: 10.1016/j.jconrel.2012.04.009
- [48] Davoren M, Herzog E, Casey A, Cottineau B, Chambers G, Byrne HJ, Lyng FM. In vitro toxicity evaluation of single walled carbon nanotubes on human A549 lung cells. *Toxicology in Vitro*. 2007;**21**:438-448. DOI: 10.1016/j.tiv.2006.10.007
- [49] Tenzer S, Docter D, Kuharev J, Musyanovych A, Fetz V, Hecht R, Schlenk F, Fischer D, Kiouptsi K, Reinhardt C, Landfester K, Schild H, Maskos M, Knauer SK. Rapid formation of plasma protein corona critically affects nanoparticle pathophysiology. *Nature Nanotechnology*. 2013;**8**:772-781. DOI: 10.1038/nnano.2013.181
- [50] Maiorano G, Sabella S, Sorce B, Brunetti V, Malvindi MA, Cingolani R, Pompa PP. Effects of cell culture media on the dynamic formation of protein-nanoparticle complexes and influence on the cellular response. *ACS Nanotechnology*. 2010;**4**:7481-7491. DOI: 10.1021/nn101557e
- [51] Ritz S, Schöttle S, Kotman N, Baier G, Musyanovych A, Kukarev J, Landfester K, Schild H, Jahn O, Tenzer S, Mailänder V. Protein corona of nanoparticles: Distinct proteins regulate the cellular uptake. *Biomacromolecules*. 2015;**16**:1311-1321. DOI: 10.1021/acs.biomac.5b00108
- [52] Urbas K, Jedrzejczak-Silicka M, Rakoczy R, Zaborski D, Mijowska E. Effect of GO-Fe₃O₄ and rotating magnetic field on cellular metabolic activity of mammalian cells. *Journal of Biomaterials Applications*. 2016;**30**:1392-1406. DOI: 10.1177/0885328216628762
- [53] Gunawan C, Lim M, Marquis CP, Amal R. Nanoparticle-protein corona complexes govern the biological fates and function of nanoparticles. *Journal of Materials Chemistry B*. 2014;**2**:2060-2083. DOI: 10.1039/C3TB21526A
- [54] Lesniak A, Fenaroli F, Monopoli MP, Åberg C, Dawson KA, Salvati A. Effects of the presence or absence of a protein corona on silica nanoparticle uptake and impact on cells. *ACS Nano*. 2012;**6**:5845-5857. DOI: 10.1021/nn300223w
- [55] Sacchetti C, Motamedchaboki K, Magrini A, Palmieri G, Mattei M, Barnardini S, Rosato N, Bottini N, Bottini M. Surface polyethylene glycol conformation influences the protein corona of polyethylene glycol-modified single-walled carbon nanotubes: Potential implications on biological performance. *ACS Nano*. 2013;**7**:1974-1989. DOI: 10.1021/nn400409h
- [56] Gaucher G, Asahina K, Wang J, Leroux JC. Effect of poly(N-vinyl-pyrrolidone)-block-poly(D,L-lactide) as coating agent on the opsonisation, phagocytosis, and pharmacokinetics of biodegradable nanoparticles. *Biomacromolecules*. 2009;**10**:408-416. DOI: 10.1021/bm801178f

- [57] Zhao Y, Wang L, Wang Q, Tang W, She Z, Deng Y. Repeated injection of PEGylated solid lipid nanoparticles induces accelerated blood clearance in mice and beagles. *International Journal of Nanomedicine*. 2012;**7**:2891-2900. DOI: 10.2147/IJN.S30943
- [58] Mijowska E, Cendrowski K, Brylak M, Konicki W. Sandwich-like mesoporous silica flakes for anticancer drug transport-synthesis, characterization and kinetics release study. *Colloids and Surfaces B: Biointerfaces*. 2015;**136**:119-125. DOI: 10.1016/j.colsurfb.2015.09.007
- [59] Peruzynska M, Szelong S, Trzeciak K, Kurzawski M, Cendrowski K, Brylak M, Roginska D, Piotrowska K, Mijowska E, Drozdziak M. In vitro and in vivo evaluation of sandwich-like mesoporous silica nanoflakes as promising anticancer drug delivery system. *International Journal of Pharmaceutics*. 2016;**506**:458-468. DOI: 10.1016/j.ijpharm.2016.03.041
- [60] Pelmenchikov A, Leszczynski J, Pettersson LGM. Mechanism of dissolution of neutral silica surfaces: Including effect of self-healing. *The Journal of Physical Chemistry A*. 2012;**24**:1462-1471. DOI: 10.1021/jp011820g
- [61] Yamada H, Urata C, Aoyama Y, Osada S, Yamauchi Y, Kuroda K. Preparation of colloidal mesoporous silica nanoparticles with different diameters and their unique degradation behaviour in static aqueous systems. *Chemistry of Materials*. 2012;**(8)**:1462-1471. DOI: 10.1021/cm3001688
- [62] Chen K, Zhang J, Gu H. Dissolution from inside: A unique degradation behaviour of core-shell magnetic mesoporous silica nanoparticles and the effect of polyethyleneimine coating. *Journal of Materials Chemistry*. 2012;**22**:22005-22012. DOI: 10.1039/c2jm34364a
- [63] Augustyniak A, Cendrowski K, Nawrotek P, Brylak M, Mijowska E. Investigating the interaction between *Streptomyces* sp. and titania/silica nanospheres. *Water Air Soil Pollution*. 2016;**227**:230. DOI: 10.4172/2157-7439.1000182
- [64] Biolog2. Phenotype MicroArrays for Mammalian Cells [Internet]. 2013. Available from: <http://www.biolog.com/pdf/pmmlit/00A%20046rA%20PM-M%20brochure.pdf> [Accessed: 2017-09-06]
- [65] Larson B, Rieger L, Travis J, Wiater L. Label-Free Phenotype MicroArrays™ Analysis of Cellular Energetic and Apoptotic Activity using Microplate Reading and Phase Contrast Imaging [Internet]. 2015. Available from: <https://www.biotek.com/resources/presentations/label-free-phenotype-microarray-analysis-of-cellular-energetics-and-apoptotic-activity-using-microplate-reading-and-phase-contrast-imaging/> [Accessed: 2017-08-21]
- [66] Biolog1. Phenotype MicroArrays™ PM-M TXO1 MicroPlate™ for Measuring Chemosensitivity Phenotypes of Mammalian Cells and for Sensitively Detecting Mitochondrial Toxicity. [Internet]. 2010. Available from: <http://www.biolog.com/pdf/pmmlit/00P%20219%20PMM%20Tox1%20MicroPlate%20100707.pdf> [Accessed: 2017-09-06]
- [67] Biolog3. Phenotype MicroArrays for Mammalian Cells (PM-M) [Internet]. 2017. Available from: http://www.biolog.com/products-static/phenotype_mammalian_cells_overview.php [Accessed: 2017-09-06]

- [68] Bochner BR, Siri M, Hunag RH, Noble S, Lei XH, Clemons PA, Wagner BK. Assay of the multiple energy-producing pathways of mammalian cells. *PLoS One*. 2011;**6**:e18147. DOI: 10.1371/journal.pone.0018147
- [69] Žigon P, Mrak-Poijsak K, Lakota K, Terčelj M, Čučnik S, Tomsie M, Sodin-Semrl S. Metabolic fingerprints of human primary endothelial and fibroblast cells. *Metabolomics*. 2016;**12**:92. DOI: 10.1007/s11306-016-1024-7
- [70] Parmar N, Wetton N, Alvarado S, Kennedy S. Profiling of human normal and cancer cell lines using phenotype microarray analysis. *FASEB Journal*. 2014;**28**:613.5
- [71] Martinez-Reyes I, Diebold LP, Kong H, Scheiber M, Huang H, Hensley CT, Mehta MM, Wang T, Santos JH, Woychnik R, Dufour E, Spelbrink JN, Weinberg SE, Zhao Y, DeBerardinis RJ, Chandel NS. TCA cycle and mitochondrial membrane potential are necessary for diverse biological functions. *Molecular Cell*. 2016;**61**:199-209. DOI: 10.1016/j.molcel.2015.12.002
- [72] Wiater LA, Naoble S, Bochner BR. Profiling Toxic Chemical with a New Liver Cell-based Assay [Internet]. 2017. Available from: http://www.biolog.com/pdf/pmmilit/Poster_AASLD_2011_PM-M_Toxt1_Assay.pdf [Accessed: 2017-09-06]
- [73] Bochner BR. New technologies to assess genotype–phenotype relationships. *Nature Reviews Genetics*. 2003;**4**:309-314. DOI: 10.1038/nrg1046
- [74] Nierode GJ, Perea BC, McFarland SK, Pascoal JF, Clark DS, Schaffer DV, Dordick JS. High-throughput toxicity and phenotypic screening of 3D human neural progenitor cell culture on a microarray chip platform. *Stem Cell Reports*. 2016;**7**:970-982. DOI: 10.1016/j.stemcr.2016.10.001
- [75] xCelligence. xCelligence RTCA DP Instrument. Flexible Real-Time Cell Monitoring [Internet]. 2014. Available from: <https://www.aceabio.com/products/rtca-dp/> [Accessed: 2016-10-09]
- [76] Phase Holographic Imaging. Holomonitor Application Note on Label-free Cell Motility. [Internet]. 2015. Available from: <http://www.phiab.se/reports/2014/CellMotilityAppNotePHI-140919.pdf> [Accessed: 2016-03-20]
- [77] Székács I, Fejes Á, Klátyik T, Patkó D, Pomóthy J, Mörtl M, Horváth R, Madarász E, Dervas B, Székács A. Environmental and toxicological impacts of glyphosate with its formulating adjuvant. *International Journal of Biological Veterinary Agricultural and Food Engineering*. 2014;**8**:219-224
- [78] Peter B, Nador J, Juhasz K, Dobos A, Korosi L, Székács I, Patko D, Horváth R. Incubator proof miniaturized holomonitor to in situ monitor cancer cells expose to green tea polyphenol and preosteoblast cells adhering on nanostructure titanate surfaces: Validity of the measured parameters and their corrections. *Journal of Biomedical Optics*. 2015;**20**:067002. DOI: 10.1117/1.JBO.20.6.067002
- [79] El-Schich Z, Kamlund S, Janickie B, Alm K, Gjörloff Wingren A. Holography: The usefulness of digital holographic microscopy for clinical diagnostics. In: Naydenova I,

Nazarova D, Babeva T, editors. Holographic Materials and Optical Systems. Rijeka: InTech; 2017. pp. 319-333. DOI: 10.5772/63255

- [80] Kim K, Yoon J, Shin S, Lee SY, Yang SA, Park YK. Optical diffraction tomography techniques for the study of cell pathophysiology. *Journal of Biomedical Photonics & Engineering*. 2016;**2**:1-16. DOI: 10.18287/JBPE16.02.020201
- [81] Mölder A, Sebesta M, Gustafsson M, Gisselson L, Gjörlöf Wingren A, Alm K. Non-invasive, label-free cell counting and quantitative analysis of adherent cells using digital holography. *Journal of Microscopy*. 2008;**232**:240-247. DOI: 10.1111/j.1365-2818.2008.02095.x
- [82] Lajkó E, Spring S, Láng O, Ingebrandt S, Mezö G, Köhidai L. Impedance-based analysis and holographic phase imaging of the GnRH-III-based drug-targeting in melanoma cells. In: *Impedance-Based Cellular Assays (IBCA'16)*; 9-12 August 2016; Regensburg, Germany. p. T20
- [83] Dudziak M. Opracowanie syntezy wytwarzania nanostruktur złota i heksagonalnego azotku boru do zastosowań biomedycznych [Thesis]. Szczecin: West Pomeranian University of Technology; 2017
- [84] Kalbac M, Kalbacova M, Broz A, Kong J. Graphene substrates promote adherence of human osteoblast and mesenchymal stromal cell. *Carbon*. 2010;**48**:4323-4329. DOI: 10.1016/j.carbon.2010.07.045
- [85] Matusiak P. Określenie właściwości mechanicznych komórek MAC-T za pomocą AFM [Thesis]. Szczecin: West Pomeranian University of Technology; 2014
- [86] Liu D, Wang L, Wang Z, Cuschieri A. Magnetoporation and magnetolysis of cancer cells via carbon nanotubes induced by rotating magnetic fields. *Nano Letters*. 2012;**12**:5117-5121. DOI: 10.1021/nl301928z

IntechOpen

